Published in final edited form as:

*IEEE Trans Ultrason Ferroelectr Freq Control*. 2019 February ; 66(2): 318–339. doi:10.1109/TUFFC.2018.2886067.

# Considerations for Choosing Sensitive Element Size for Needle and Fiber-Optic Hydrophones I: Spatiotemporal Transfer Function and Graphical Guide

**Keith A. Wear [Senior Member, IEEE]**

Center for Devices and Radiological Health, Food and Drug Administration, Silver Spring, MD, 20993 USA

## Abstract

The spatiotemporal transfer function for a needle or reflectance-based fiber-optic hydrophone is modeled as separable into the product of two filters corresponding to frequency-dependent sensitivity and spatial averaging. The separable hydrophone transfer function model is verified numerically by comparison to a more general rigid piston spatiotemporal response model that does not assume separability. Spatial averaging effects are characterized by frequency-dependent "effective" sensitive element diameter, which can be more than double the geometrical sensitive element diameter. The transfer function is tested in simulation using a nonlinear focused pressure wave model based on Gaussian harmonic radial pressure distributions. The pressure wave model is validated by comparing to experimental hydrophone scans of nonlinear beams produced by three source transducers. An analytic form for the spatial averaging filter, applicable to Gaussian harmonic beams, is derived. A second analytic form for the spatial averaging filter, applicable to quadratic harmonic beams, is derived by extending the spatial averaging correction recommended by IEC 62127-1 Annex E to nonlinear signals with multiple harmonics. Both forms are applicable to all hydrophones (not just needle and fiber optic hydrophones). Simulation analysis performed for a wide variety of transducer geometries indicates that the Gaussian spatial averaging filter formula is more accurate than the Quadratic form over a wider range of harmonics. Additional experimental validation is provided in Part II. Readers who are uninterested in hydrophone theory may skip the theoretical and experimental sections of this paper and proceed to the Graphical Guide for practical information to inform and support selection of hydrophone sensitive element size (but might be well-advised to read the Introduction).

### Keywords

Acoustic output measurement; hydrophone; needle; fiber optic; spatial averaging; spatiotemporal transfer function

*Corresponding author: Keith A. Wear*. keith.wear@fda.hhs.gov.

## I. Introduction

Measurement of acoustic output is important for characterizing safety and effectiveness of medical ultrasound devices and for rigorously documenting ultrasound experiments. An ultrasound wave can be detected with a hydrophone, which senses the pressure distribution incident on its sensitive element and produces an output voltage [1-3]. Hydrophones unfortunately produce distorted versions of incident pressure waves. This distortion arises from two main factors: frequency-dependent sensitivity and spatial averaging across the sensitive element. The main objectives of this paper are 1) to provide a guide for the effect of sensitive element size on distortion of pressure measurements of nonlinear ultrasound signals performed with needle and fiber-optic hydrophones and 2) to provide inverse filters to correct for this distortion.

Needle and fiber optic hydrophones have many applications in medical ultrasound and non-destructive evaluation. Needle hydrophones are less expensive and more compact than membrane hydrophones and are often used for characterization of transcranial [4-11], high-intensity therapeutic [12-14], and gene-delivery [15] systems. They are also used for high-frequency transducer characterization [16], cavitation detection [17], and other medical applications [18, 19]. Reflectance-based fiber optic hydrophones can withstand very high pressures (*e.g.*, up to 70 MPa and beyond [20-23]) and have been used for high-intensity therapeutic ultrasound (HITU) [13, 20-28] and lithotripsy [29] applications.

Sensitive element size affects both sensitivity and spatial averaging. As sensitive element size increases, sensitivity tends to increase but spatial averaging artifacts also tend to increase. Needle and fiber-optic hydrophones come in a wide variety of sensitive element sizes ranging from 7 μm [24] to 1 mm and above, making the choice difficult. This guide will help researchers make appropriate choices for hydrophone sensitive element size for their experiments and compensate measurements for distortion if necessary.

The first main factor responsible for hydrophone distortion is frequency-dependent sensitivity, $M_L(f)$, which is defined as

$$M_L(f) = \frac{V(f)}{P_{NP}(f)} \tag{1}$$

where $V(f)$ is the hydrophone voltage output at a temporal frequency $f$ and $P_{NP}(f)$ is the pressure of a normally-incident ultrasound wave that appears quasi-planar across the sensitive element. Sensitivity depends on frequency, resulting in a filtering effect on the input waveform. The amount of distortion is related to the degree of frequency dependence of hydrophone sensitivity over the band of frequencies in the incident pressure spectrum. This is a concern for nonlinear pressure signals that contain multiple harmonics that can span many MHz or even tens of MHz (*e.g.*, for HITU). Some investigations have shown that distortion of quasi-planar pressure waves due to frequency-dependent hydrophone sensitivity can be substantially mitigated by deconvolution of sensitivity from the measured voltage signal [14, 30-36].

The second main factor responsible for hydrophone distortion is spatial averaging across the sensitive element [37-46]. Some investigations have shown that distortion of quasi-linear pressure waves due to spatial averaging can be mitigated by spatial deconvolution of the receiver aperture function from the measured voltage signal [43, 44].

The problem becomes more challenging for signals that are neither quasi-planar nor quasi-linear. Nonlinear beams have 1) broad bandwidths that lead to frequency-dependent sensitivity artifacts and 2) high-frequency content in harmonics that is susceptible to spatial averaging artifacts.

Most investigations of hydrophone distortion consider either frequency-dependent sensitivity [30-36] or spatial averaging [37-41, 43, 44, 46-48] but not both. For cases when both distortions are significant, it would be convenient if the two distortions could be considered independently so that, for example, one deconvolution could be performed first and then the second deconvolution afterward. This approach implicitly assumes that the hydrophone spatiotemporal response, $H_p(f)$, is separable into a product of two factors arising from frequency-dependent sensitivity and spatial averaging.

$$H_p(f) = M_L(f)S_p(f) \tag{2}$$

where $S_p(f)$ is a spatial averaging filter. The subscript $p$ is a reminder that a function depends on the particular spatiotemporal pressure field distribution.

The present paper investigates the validity of the separable form of the spatiotemporal response through comparison to a theoretical rigid piston hydrophone spatiotemporal response [49, 50] that does not assume separability and has been validated for predicting sensitivity [51, 52] and directivity [53] of needle hydrophones and sensitivity [52] and directivity [54] of reflectance-based fiber-optic hydrophones. This paper is relevant to reflectance-based fiber optic hydrophones that measure changes in a fluid refractive index caused by pressure changes [20, 25, 54-57]. This paper does not consider fiber optic displacement sensors [58]. Fabry-Perot interferometic fiber optic hydrophones [33, 59-62], other Fabry-Perot sensors [63], or other fiber optic designs [64-66]. A formula for the frequency-dependent “effective” sensitive element diameter, which determines spatial averaging effects, is obtained from the theoretical directivity. The framework can be applied to pressure fields with circular or rectangular symmetry. Calculations are performed here more fully for circularly-symmetric fields but suggestions are made for how to extend the framework for rectangularly-symmetric fields. Although analytic analysis is easier for circularly-symmetric fields, numerical analysis based on this framework is straightforward with either symmetry. The theoretical spatiotemporal response is tested in simulation using a focused pressure wave model, which is itself validated by comparison to hydrophone measurements of acoustic output from three source transducers.

This paper also presents a new model for spatial averaging effects due to integration of the pressure wave across the hydrophone sensitive element. This model is applicable for many hydrophone designs, not just needle and reflectance-based fiber optic hydrophones but also membrane and capsule hydrophones if their frequency-dependent sensitive element size is

known from separate measurements or modeling. This expression offers advantages over the method recommended in IEC 62127-1 Annex E, including 1) it provides an analytic expression for the spatial averaging filter, 2) it does not require a separate off-axis measurement of pressure, and 3) it does not assume a quadratic radial pressure distribution that limits applicability roughly to within the full width half maximum (FWHM) of the beam. This last feature allows greater extension to high frequency fields, whether generated by a high fundamental frequency or harmonics of a low fundamental frequency (in the case of HITU).

Finally, this paper offers a graphical guide to help investigators choose and defend hydrophone sensitive element size for their experiments.

## II. Theory

### A. Rigid Piston Model for Needle and Fiber Optic Hydrophones

The rigid piston (RP) model [49, 50] has been validated for predicting sensitivity [51, 52] and directivity [53] of many needle hydrophones and sensitivity [52] and directivity [54] of a reflectance-based fiber optic hydrophone. One RP model expresses spatiotemporal response in the form of an integral that may be evaluated numerically [50]. The theory does not simply perform a spatial average of the free-field pressure across the sensitive element of the hydrophone. Rather, it accounts for the fact that the hydrophone perturbs the pressure field by imposing a boundary condition that the component of velocity normal to the sensitive element must be zero (rigid piston assumption).

When the angle of incidence for an incoming plane wave is zero, the RP model describes frequency-dependent sensitivity in the absence of spatial averaging and reduces to

$$H_{RP}(f,\theta=0)=2-\frac{1}{\pi a_2^2}\int_0^{2\pi}\int_0^{a_2} e^{-i2\pi f b(r,\phi)/c} r\,dr\,d\phi \tag{3}$$

where $f$ = frequency, $c$ = sound speed in the fluid, $a_2$ = sensitive element radius (*e.g.*, fiber optic cable core), $a_1$ rigid piston radius (*e.g.*, core plus cladding) and

$$b(r,\phi)=\sqrt{r^2\cos^2\phi+(a_1^2-r^2)}-r\cos\phi\,. \tag{4}$$

Fig. 1 illustrates the zero-angle transfer function and shows its effect on a quasi-planar tone burst. The zero-angle transfer function is a high pass filter up to a maximum response frequency at $f_{max}=1.2c/(\pi a_g)$, where the hydrophone geometrical sensitive element radius $a_g=a_1=a_2$. In Fig. 1, $a_g$ = 150 μm and therefore $f_{max}$ = 3.8 MHz. The high pass filter boosts harmonics relative to the fundamental, resulting in higher, sharper compressional peaks and lower, more rounded rarefactional peaks [52]. A needle hydrophone model, which accounts not only for diffraction but also for multiple reflections within the layered structure of polyvinylidene fluoride (PVDF), predicts similar frequency dependence for sensitivity [67].

The full RP model provides $H_{RP}(f, \theta)$ as the sum of two integral expressions that may be evaluated numerically [50]. For brevity, the mathematics is not reproduced here. Note that $H_{RP}(f, \theta)$ mathematically describes the effects of integration of the pressure field across the sensitive element and is dimensionless while $H_p(f)$ in (2) has dimensions of voltage divided by pressure (*e.g.*, V/MPa).

## B. Effective Sensitive Element Size

A pressure field incident upon a hydrophone may be decomposed into an angular spectrum of plane waves incident upon the sensitive element. The dependence of hydrophone response on angle of incidence is called directivity. Spatial averaging is zero for normally incident plane waves and monotonically increases with angle of incidence. Therefore, spatial averaging effects are related to hydrophone directivity.

Empirical studies suggest that spatial averaging effects may be accurately predicted by integrating the free field (that is, the field in the absence of a hydrophone) over the surface of an imaginary hydrophone sensitive element with an appropriate "effective" sensitive element size [45, 68]. The effective sensitive element radius $a_{\text{eff}}$ can differ from the geometrical sensitive element radius $a_g$ and can depend on frequency.

IEC 62127-3 Section 5.6 recommends estimation of $a_{eff}(f)$ by fitting directivity measurements for a circular receiver to the rigid baffle (RB) directivity model [1]

$$D_{RB}(k, \theta) = \frac{2J_1(kasin\theta)}{kasin\theta} \tag{5}$$

where $k = 2\pi / \lambda$, $\lambda$ is wavelength, $a$ is sensitive element radius (adjustable fitting parameter), and $\theta$ is the angle of an incident plane wave [68]. There are multiple methods for measuring directivity [45, 53, 54, 69-72]. The RB-model approximation may be useful for needle and fiber optic hydrophones because it offers an expedient alternative to numerical evaluation of the integral form of the RP model [50]. However, the RB-model approach requires knowledge of $a_{eff}(f)$. In the present paper, $a_{eff}(f)$ will be designated as the value of $a$ in (5) that gives the minimum least-squares difference between an RB directivity with $a=a_{eff}(f)$ and an RP directivity with $a_1=a_2=a_{\text{g}}$. The RB directivity based on $a_{eff}(f)$ will be compared with directivity predictions obtained directly from the RP model based on $a_1=a_2=a_{\text{g}}$ in order to evaluate the validity of the expedient RB approach.

## C. Parametric Model for Nonlinear, Focused Beam: Temporal Dependence

An analytic expression for the spatiotemporal pressure distribution will be useful for predicting hydrophone filtering effects for some practical pressure measurement tasks. In this section, a form for pressure will be derived for a circularly-symmetric transducer. A previous investigation [52] showed that, for the purpose of investigating distortions due to frequency-dependent sensitivity of a rigid cylinder hydrophone, the temporal dependence of pressure may be accurately modeled using the formula of Ayme and Carstensen [73], modified according to the model of Zeqiri and Bond [40] that incorporates coefficients, $B_{\text{n}}(\sigma)$, derived by Blackstock [74] to describe weights for harmonics. The real part of a

circularly symmetric pressure field can be denoted by $p_{real}(r, t)$. The real part of the axial field is given by

$$p_{real}(r=0,t)=\sum_{n=1}^{N} B_n(\sigma)\sin\left(2\pi n f_1 t+\frac{\pi}{4}\right) \tag{6}$$

where $f_1$ = the fundamental frequency. For the shock-free region, $0 \leq \sigma < 1$, $B_n(\sigma) = (2/n\sigma)J_n(n\sigma)$ ("Fubini solution" [74]). More generally,

$$B_n(\sigma)=\left(\frac{2}{n\pi}\right)\left\{V_b+\frac{1}{\sigma}\int_{\Phi_{min}}^{\pi} cos[n(\Phi-\sigma sin\Phi)]d\Phi\right\} \tag{7}$$

where shock amplitude $V_b = \sin\Phi_{min} = \sin(\sigma V_b)$. Blackstock's theory was derived for plane waves. This paper will provide experimental tests for the extension of Blackstock's $B_n(\sigma)$ coefficients to model spectral weights for focused beams. In complex phasor notation,

$$p(r=0,t)=\sum_{n=1}^{N} B_n(\sigma)\exp\left[i\left(2\pi n f_1 t-\frac{\pi}{4}\right)\right] \tag{8}$$

where $p_{real}(r, t) = \mathrm{Re}\,[\,p(r, t)\,]$ and the identity $\cos(\varphi) = \sin(\varphi + \pi/2)$ has been used. The temporal Fourier transform of $p(r=0, t)$ is

$$P(r=0,f)=exp\left(-i\frac{\pi}{4}\right)\sum_{n=1}^{N} B_n(\sigma)\delta(f-nf_1) \tag{9}$$

where $\delta(f)$ is the Dirac delta function.

Finite pulse duration effects could be modeled by multiplying $p(r=0, t)$ by a time-dependent envelope function, $m(t)$, as previously [52]. However, this added complication would not add much practical value to the model when tone bursts are investigated, as the following discussion will argue. The effects of finite pulse duration would be to replace the delta function, $\delta(f - nf_1)$, in (9) with the Fourier transform of the envelope function, $M(f) = \mathcal{F}[m(t)]$, giving each spectral lobe, $M(f - nf_1)$, a finite width in frequency domain ($\Delta f_m$) inversely proportional to the temporal duration of the envelope ($\Delta t_m$) so that $\Delta f_m = 1/\Delta t_m$. Fig. 2 illustrates the justification for retaining the simple harmonic delta function spectrum in (9). Fig. 2a shows a sensitivity filter (red dashed line) and a spatial averaging filter (blue solid line). Fig. 2b shows a general spectrum with finite-width harmonics (red dotted line) and a simple harmonic delta function approximation (vertical blue lines). Validity of the simple harmonic delta function approximation requires that the sensitivity and spatial averaging filters do not vary greatly across the width of a harmonic lobe in the true spectrum. This assumption will be satisfied by many practical examples in nonlinear medical ultrasound when tone bursts are used. For example, pulses of durations of 1 μs or more will have spectral lobes of width on the order of 1 MHz or less, which is less than the scale of significant variation of 1) sensitivities of needle and fiber optic hydrophones with sensitive element diameters in the range of 100 μm to 600 μm [52] and 2) spatial averaging

correction factors for a 150 μm diameter hydrophone measuring pressure from acoustic sources with f-numbers in the range of 3.84 to 19 [47]. This assumption will be tested for hydrophone diameters ranging from 200 μm to 1000 μm and acoustic source f-numbers ranging from 1.4 to 2.0 in the sequel to this paper, which will provide experimental validation for this model [75].

### D. Parametric Model for Nonlinear, Focused Beam: Spatiotemporal Dependence

Prediction of spatial averaging effects will require a model for the radial dependences of harmonic pressure waves. Now assume that each harmonic component is separable into the product of axial and radial components [76].

$$p(r,t) = \sum_{n=1}^{N} B_n(\sigma) \exp\left[i\left(2\pi n f_1 t - \frac{\pi}{4}\right)\right] w_n(r) \tag{10}$$

where $r$ is the radial coordinate and $w_n(r)$ gives the radial dependence of the complex beam for the $n^{th}$ harmonic. Note that the axial temporal dependence is similar to an expression given by Muir and Carstensen for a converging spherical wave (Equation 7 in [77]). However, the radial dependence is different in that it results in a form for $p(r, t)$ that is separable in cylindrical coordinates, which is convenient for modeling spatial averaging effects with hydrophones.

A Gaussian form will be employed to model $w_n(r)$

$$w_n(r) = exp(i\, g_n\, r^2) exp\left[-\frac{r^2}{2\sigma_n^2}\right] \tag{11}$$

This Gaussian form is assumed to be a good approximation within the range of $r$ corresponding to the spatial extent of the hydrophone sensitive element. The coefficient $g_n$ is related to the rate of phase change with the radial coordinate. The FWHM of each harmonic component is $\sigma_n 2\sqrt{2ln2}$ (where $\sigma_n$ should not be confused with Blackstock's $\sigma$). Fig. 3 compares a Gaussian form for the fundamental frequency component with the quadratic form used in the IEC 62127-1 Annex E spatial averaging method. Both forms are quite close to the theoretical diffraction pattern for a circular, concave piston transducer at radial coordinate $r <$ the half width half maximum (HWHM) of the focused beam. For pressure fields with rectangular symmetry, (11) could be adapted by replacing $g_n r^2$ in the first factor by $g_{nx}x^2+g_{ny}y^2$ and by replacing $r^2 / \sigma_n^2$ in the second factor by $x^2 / \sigma_{nx}^2 + y^2 / \sigma_{ny}^2$.

One advantage of the Gaussian form over the quadratic form used in IEC 62127-1 Annex E is that as the radial coordinate $r$ increases, the pressure amplitude goes to zero rather titan $-\infty$, which makes more sense physically. The quadratic form was not intended for nonlinear ultrasound beams and is adequate for a fundamental component when the hydrophone sensitive element diameter is much smaller than the FWHM of the beam, as it should be. However, nonlinear beams will contain multiple harmonics with beam widths decreasing as harmonic number increases. The Gaussian form allows for more realistic asymptotic

behavior of harmonic components than the quadratic form. A second advantage of the Gaussian form is that it has a straightforward spatial two-dimensional Fourier transform (*i.e.,* another Gaussian) that corresponds to an angular spectrum of plane wave components. This makes it compatible with the RP model, which represents the hydrophone spatiotemporal transfer function in terms of response to incident plane waves as a function of angle of incidence. A third advantage of the Gaussian form is that it leads to an analytic form for the spatial averaging correction (see next section). Gaussian representations have been shown to be useful for modeling moderately nonlinear HITU pulses that contain many acoustical cycles [76]. The present paper will provide experimental validation for the Gaussian harmonic beam approximation for three circular focused piston transducers in the focal plane.

This approach resembles previous efforts to model nonlinear Gaussian beams [76, 78, 79]. It is important to note, however, that previous theories assume a Gaussian source (unlike the present approach). Those theories predict beam properties over an extended range of propagation distance. The present approach is only valid where a beam may be approximated as a Gaussian, which, in the case of a circular focused piston source, may limit it to near the focal region [80]. The fundamental diffraction pattern from a circular focused piston source departs from Gaussian shape beyond the FWHM, but this is also true for the quadratic form used in IEC 62127-1 Annex E. See Fig. 3. Some theories solve for a complex multiplicative factor that depends on axial propagation distance but not on radial position. This factor is important for modeling axial variations as in [76] but is not required here since only a measurement plane perpendicular to the propagation direction is of interest.

Now the task is to obtain forms for $g_n$ and $\sigma_n$ in (11) in terms of experimental geometrical parameters. These may be obtained theoretically, numerically, or experimentally by fitting Gaussian functions to harmonic beam radial profiles. One useful case to consider is the pressure field distribution in the focal plane of a circular focused piston transducer. For $n = 1$, a Gaussian form may be fit to the radial dependence of the theoretical diffraction pattern [81],

$$w_1(r) \approx exp\left(ik_1 \frac{r^2}{2D}\right) \frac{2J_1(k_1 a_s r/D)}{k_1 a_s r/D} \tag{12}$$

where $k_1 = 2\pi/\lambda_1$, $\lambda_1 = c/f_1$, $c$ = speed of sound, $a_s$ = the radius of the source, and $D$ = the focal length of the source. The $2J_1(\pi x)/(\pi x)$ function is sometimes called the jinc, besinc, or sombrero function. For pressure fields with rectangular symmetry, (12) could be adapted by replacing $r^2$ in the phase factor by $x^2 + y^2$ and replacing the jinc function with the product of two orthogonal sinc functions where sinc(x) = sin(x) / x (see section 4-2 in [82]). This theory has been validated in the focal plane and along the transducer axis throughout an extensive range in the axial dimension [81]. However, it should be noted that for sufficiently intense beams, the shape of the radial distribution for the fundamental component can become distorted due to preferential loss of energy (that is, conversion to higher harmonics) from the center of the beam, where the intensity is highest [83]. In addition, for sufficiently high source pressures, shocks can form prefocally, resulting in wider focal beam widths [21, 84].

In the present paper, the magnitude of this beam distortion will be investigated by solving the Khokhlov-Zabolotskaya-Kuznetsov (KZK) equation numerically for a variety of circular focused piston transducer parameters and levels of nonlinearity. The set of conditions under which (12) is valid for the fundamental radial pressure distribution will be referred to as classic-jinc-fundamental (CJF) conditions to distinguish them from general Gaussian (GG) conditions that do not assume (12).

The validity of (12) becomes increasingly challenged as f-number (F# = ratio of focal distance to aperture diameter) decreases [85, 86]. Table I tests criteria for validity [81] of (12) for an F/1 transducer with frequency and dimensions typical for therapeutic applications, such as the Sonic Concepts (Bothell, WA) H-101. The criteria are mostly met, except the third criterion at 3.3 MHz. Nevertheless, Table I shows that (12) predicts FWHM consistent with values obtained by simulation [87] and experiment [14]. For smaller f-numbers, alternative diffraction models may be required [85, 86].

A form for $g_1$ in (11) for a circular focused piston transducer under CJF conditions may be found by comparison of phase factors in (11) and (12), which results in $g_1 = k_1 / 2D$. The phase factor may be extended to higher harmonics by using the form from quasi-linear Gaussian beam propagation theory [76], resulting in $g_n = n\, k_1 / 2D$. This assumption might seem to limit the model to quasi-linear conditions. However, as will be shown in the next section, it is plausible that for typical transducers, magnitude considerations are far more important than phase considerations for predicting spatial averaging effects. Therefore, the quasi-linear phase assumption may not limit the model severely. Note that the IEC 62127-1 Annex E spatial averaging correction, which is based on work by Preston *et al.* [38], ignores phase effects altogether. The validity of the phase model will be tested experimentally in a companion paper [75].

A form for $\sigma_1$ in (11) for a circular focused piston transducer under CJF conditions may be found by minimizing the mean-square difference between the magnitudes of (11) and (12) over the HWHM of the beam, which results in $\sigma_1 = 1.93\ D / (k_1 a_s)$ in the focal plane. The magnitude factor may be extended to higher harmonics by postulating that $\sigma_n = \sigma_1 / n^q$. This harmonic-dependent beam width model has been applied empirically to measurements of nonlinear ultrasound beams, with a measurement of $q = 0.61$ [88]. In the quasi-linear limit for Gaussian sources, $q = 0.5$ [76, 78, 79]. Under CJF conditions, $\sigma_n = 1.93\ D / (n^q\, k_1 a_s)$. This paper will provide results of KZK-equation simulations and experiments to 1) identify conditions when a power law is appropriate to model the dependence of harmonic beam width on harmonic number and 2) determine appropriate values for $q$.

As stated previously, the variant of the RP model used here gives the rigid piston response to an incident plane wave as a function of temporal frequency and plane wave angle of incidence. Therefore, it is helpful to decompose each harmonic component into its angular spectrum, which is given by the two-dimensional Fourier transform (which for a field with circular symmetry is also the Fourier-Bessel or Hankel transform) of $w_n(r)$. In order to accomplish this, it is useful to express the radial dependence of harmonic pressure as

$$w_n(r) = exp\left[-\frac{{b_n}^2 r^2}{2}\right] \tag{13}$$

where

$${b_n}^2 = \frac{1}{\sigma_n^2} - i2g_n \tag{14}$$

The CJF form for $\sigma_n$ may be used if appropriate. Otherwise, $\sigma_n$ may be obtained from theory, simulation, or experiment. The Fourier-Bessel transform of each harmonic component of the Gaussian beam is given by

$$W_n(\rho) = \frac{2\pi}{b_n^2} exp\left[-\frac{(2\pi\rho)^2}{2b_n^2}\right] \tag{15}$$

This expression gives weighting factors for plane wave components of the $n^{\text{th}}$ harmonic as a function of spatial frequency, $\rho$, or equivalently, angle of incidence, $\theta_z(\rho, f) = \cos^{-1}\left[\sqrt{1-(c\rho/nf_1)^2}\right]$ [82]. Now the complex phasor pressure field transformed to both temporal-frequency domain and angular spectrum frequency domain becomes

$$P(\rho, f) = exp\left(-i\frac{\pi}{4}\right)\sum_{n=1}^{N} B_n(\sigma)\,\delta(f - nf_c)W_n(\rho) \tag{16}$$

Finally, the spatiotemporally transformed hydrophone output voltage may be predicted by taking the product of $P(\rho, f)$ in (16) with $H_{RP}(\rho, f)$. $H_{RP}(\rho, f)$ may be obtained from $H_{RP}(\theta_z, f)$ predicted by the RP model [50] and knowledge that $\theta_z(\rho, f) = \cos^{-1}\left[\sqrt{1-(c\rho/nf_1)^2}\right]$. Time-domain signals may be obtained by inverse Fourier transformation.

## E. The Spatial Averaging Filter

The reduction of measured pressure due to spatial averaging across the hydrophone sensitive element is given by the integral of the incident pressure field divided by the effective area of the sensitive element [38, 40, 46-48]. When expressed as a spatial averaging filter with a frequency-dependent effective sensitive element size,

$$S_p(f) = \frac{\int_0^{2\pi}\int_0^{a_{eff}(f)} p(r, f) r dr d\theta}{\pi a_{eff}^2(f)} \tag{17}$$

where $a_{eff}(f)$ is the frequency-dependent hydrophone effective sensitive element radius. This applies to all hydrophones, not just rigid piston hydrophones. The integral in the numerator can be simplified if phase effects are negligible. Phase effects are negligible if, as $r$ moves

outward from the axis, the magnitude of each harmonic pressure wave falls significantly before the phase begins to deviate substantially from 0 radians. Consider the fundamental wave under CJF conditions. In the focal plane of a circular focused piston transducer, the phase of the fundamental component reaches 10° (π/18 radians) when $r = r_{10}$ or

$$\frac{k_1 r_{10}^2}{2D} = \frac{\pi}{18} \; or \; r_{10}^2 = \frac{\lambda_1 D}{18} \tag{18}$$

Meanwhile the – 6dB point in the beam occurs at $r_{-6\,\mathrm{dB}} = 0.705\ \lambda_1\ F\#$. The ratio is

$$\frac{r_{10}}{r_{-6\,dB}} = \frac{0.34}{F\#}\sqrt{\frac{D}{\lambda_1}} \tag{19}$$

So if the focal plane is many fundamental wavelengths away from the transducer ($D >> \lambda_1$) and the F# is not too large, then $r_{10} > r_{-6\,\mathrm{dB}}$ so phase does not greatly affect the integral for the fundamental component. This example suggests that it is plausible that phase effects do not greatly affect the integral for harmonics. For sufficiently high harmonic numbers, the sensitive element may encompass one or more sidelobes in addition to the main lobe of a harmonic component of the beam. Although the diffraction pattern may undergo sign changes (phase shift = π radians) at nulls surrounding sidelobes, contributions to the spatial averaging integral from sidelobes may be small compared to the contribution from the main lobe so neglecting these sign changes may not have a big effect on the spatial averaging filter. The sequel to the present paper will show experimental data to investigate the importance of the phase factor for some nonlinear beams [75].

If phase can be ignored for all harmonics, then it can be shown that for Gaussian beams (either GG or CJF conditions),

$$S_p(nf_1) = \frac{1}{\Omega_n^2}\left[1 - e^{-\Omega_n^2}\right] \tag{20}$$

where

$$\Omega_n^2 = \frac{a_{eff}^2(nf_1)}{2\sigma_n^2} \tag{21}$$

and the following indefinite integral has been used.

$$\int x e^{-vx^2}\,dx = -\frac{1}{2v}e^{-vx^2} \tag{22}$$

Again, the CJF form for $\sigma_n$ may be used if appropriate. Otherwise, $\sigma_n$ may be obtained from theory, simulation, or experiment. The spatial averaging filter may be seen to be a function of the ratio of the frequency-dependent effective size of the hydrophone to the beam width.

Recall that the FWHM of each harmonic component is $\sigma_n 2\sqrt{2\,ln2}$. As the ratio approaches infinity, $S_p(f)$ approaches zero, as expected. As the ratio approaches zero, $S_p(f)$ approaches one, as expected. (This can be seen by expanding the exponential in (20) as a Taylor series and retaining the first two terms).

## F. Extension of the Quadratic Spatial Averaging Model

Preston *et al.* derived a formula for spatial averaging based on the assumption that the radial pressure distribution near the beam axis could be approximated as quadratic [38].

$$p(r) = 1 - br^2 \tag{23}$$

This model applies to all hydrophones, not just rigid piston hydrophones, and assumes that effects due to phase are negligible. Preston *et al.* derived a formula for a spatial averaging correction factor $C$ (inverse of the spatial averaging filter) that requires one measurement on axis and another measurement one hydrophone radius off axis. Their result is

$$C = \frac{3 - \beta}{2} \tag{24}$$

where

$$\beta = \frac{signal\ at\ one\ hydrophone\ radius\ from\ the\ axis}{signal\ on\ axis} \tag{25}$$

This formula is the basis for the spatial averaging correction method in IEC 62127-1 Annex E [89]. Interestingly, it can be shown that this result holds regardless of the value of the quadratic coefficient $b$, provided the hydrophone sensitive element is small enough so that both measurements are within the zone of the beam where the radial pressure distribution may be accurately modeled as quadratic. Accordingly, Preston *et al.* did not provide a formula for $b$.

This formulation will be extended here to nonlinear pressure waves by applying (23) – (25) to each harmonic component. This can be denoted by adding the subscript $n$ to Preston *et al.*'s notation as follows: $p_n(r)$, $b_n$, $C_n$, and $\beta_n$. While Preston *et al.*'s formulation could have been applied to linear experimental hydrophone voltage signals in time or frequency domain, the nonlinear extension is probably more easily applied after Fourier transformation of time domain hydrophone voltage signals, so that harmonic magnitudes may be evaluated individually.

The harmonic extension of Preston *et al.*'s method may be used to estimate the spatial averaging filter from measurements regardless of whether CJF conditions apply. First, $\beta_n$ may be evaluated using (25) on all measureable harmonic components of Fourier transformed hydrophone voltage signals. Then, $C_n$ may be evaluated from $\beta_n$ using (24). Finally, the spatial averaging filter may be evaluated with $S_p(nf_1) = 1 / C_n$. (As with Preston *et al.*'s method, this method requires knowledge of $a_{eff}(nf_1)$, which can be obtained from

directivity measurements or theoretical considerations (see Results section). Harmonic beam widths, $\sigma_n$, can be estimated by equating the empirical and theoretical (20) spatial averaging filters. Of course, $\sigma_n$ can also be estimated from lateral hydrophone scans (see Results section).

A theoretical form for the spatial averaging filter may be derived under quadratic beam and CJF conditions, obviating the need for measurement of $\beta_n$. Although Preston *et al.* did not show this, it can be shown, by using (23) in (17), that the spatially-averaged mean value of the quadratic field corresponding to the $n^{th}$ harmonic over the hydrophone sensitive element is

$$S_p(nf_1) = 1 - \frac{b_n a_{eff}^2 (nf_1)}{2} \tag{26}$$

A formula for $b_1$ for the fundamental wave may be obtained by minimizing the mean square difference between the diffraction pattern under CJF conditions (12) and a quadratic approximation over the FWHM of the beam. The result is

$$b_1 = 0.108\left(\frac{k_1 a_s}{D}\right)^2 \tag{27}$$

Approximating the fundamental as a Gaussian under CJF conditions, the relation $\sigma_1 = 1.93\, D/(k_1 a_s)$ can be used to obtain

$$b_1 = \frac{0.402}{\sigma_1^2} \tag{28}$$

For a nonlinear Gaussian beam,

$$b_n = \frac{0.402}{\sigma_n^2} \tag{29}$$

This gives a spatial averaging filter of

$$S_p(nf_1) = 1 - \frac{0.201 a_{eff}^2 (nf_1)}{\sigma_n^2} \tag{30}$$

This formula is valid throughout the zone in which a Gaussian beam can be adequately approximated by a quadratic function or roughly for $r < \mathrm{HWHM_n} = \sqrt{2\ln 2}\,\sigma_n = 1.18\sigma_n$ (see Fig. 3). The maximum difference between a Gaussian function, $\exp(-r^2/2\sigma_n^2)$, and a least-squares quadratic fit remains below 5% for $r < 1.27\sigma_n$. This occurs for $r = a_{eff}(nf_1)$ when

$$\frac{a_{eff}(nf_1)}{\sigma_n} < 1.27 \tag{31}$$

For a beam obeying a power law dependence of beam width vs. harmonic number,

$$\frac{a_{eff}(nf_1)}{\sigma_1/n^q} < 1.27 \tag{32}$$

or

$$n^q < 1.27\frac{\sigma_1}{a_{eff}(nf_1)} \tag{33}$$

where $\sigma_n = \sigma_1 / n^q$ as discussed in Section II.D. In the focal plane of a circular, focused piston, if the fundamental lobe shape has not undergone significant nonlinear distortion, the relation $\sigma_1 = 1.93\ D / (k_1 a_s)$ can be used in (33).

Simulation analysis will be performed to compare the quadratic form of the spatial averaging correction with the more general form derived in the previous section.

## III. Methods

### A. Computation for Rigid Piston Transfer Function

Krucker *et al.* obtained an expression for the spatiotemporal transfer function of a rigid piston due to an incident plane wave as a function of frequency, angle of incidence, sensitive element radius, and the radius of a rigid outer layer surrounding the sensitive element (*e.g.*, cladding of a fiber optic hydrophone) [50]. For normally incident plane waves this expression gives similar results to those derived by Jones [49, 52].

The transfer function is the sum of two integrals. The first integral corresponds to angular-dependent averaging of the incoming plane wave due to phase cancellation over the sensitive element. This integral is the same as the RB model and is easy to compute.

The second integral corresponds to diffracted and reflected waves and is evaluated numerically. It is a double integral, one integral over the sensitive element (*e.g.*, fiber core) and another integral over the entire piston surface (*e.g.*, core plus cladding). The integrals were performed in polar coordinates of radius $r$ and angle $\phi$. For each harmonic, the radial grid spacing $\Delta r$ was set to the minimum of $a_g/10$ and $\lambda / 2.09$ where $\lambda = c / (nf_1)$. The non-integer value of 2.09 was chosen to avoid repeated samplings at the same phase of the pressure field. For each value of $r$, the angular spacing $\Delta\phi$ was initially set to $2 \tan^{-1} (\Delta r / 2r)$ to make spatial sampling consistent for radial and angular integrals. The value of $\Delta\phi$ was then reduced to the highest value below the initial value such that the angular integral would contain an integer number of angular intervals. These choices for grid spacing have been validated previously by comparison of computations with measurements of directivity of

needle [53] and fiber optic [54] hydrophones for $ka_g$ ranging from 0.4 to 21.2 and $\phi$ ranging from 0 to 90°.

Computations were performed using Matlab (Natick, MA) on a Dell notebook computer with a 2.6 GHz i7 processor with 16 GB of RAM. Computation time of the second integral increased rapidly with $ka_g$. It has been shown previously that the first integral (RB model) dominates the second integral (diffraction and reflection) for $ka_g > 4$ [53]. Therefore, in the present paper, the RB model was used to approximate the spatiotemporal transfer function for $ka_g > 8$.

## B. Approximation of Rigid Piston Transfer Function with Rigid Baffle Transfer Function with Frequency-Dependent Effective Sensitive Element Radius

Frequency-dependent hydrophone effective radius $a_{eff}(f)$ was determined by fitting the RB directivity model (5) to the reference directivity (here, the theoretical RP model instead of experimental measurements). RB model directivities, $2J_1(ka\sin\theta) / (ka\sin\theta)$, were least-squares fit to RP model predictions, $H_{RP}(\theta, f)$ (based on $a_g$), using $a$ as the adjustable fitting parameter. Root mean square differences (RMSDs) between RP and RB model directivities were computed for trial values of $a$ = 10, 20, 30, … 1000 μm. Computations were repeated for frequencies $f$ = 1, 2, 3, … 10 MHz and geometrical sensitive element radii $a_g$ = 50, 100, 150, 200, and 250 μm. For each value of frequency $f$ and geometrical sensitive element radius $a_g$, the value of $a$ that minimized RMSD was chosen for $a_{eff}(f)$. A similar approach was taken by Wilkens and Molkenstruck to estimate $a_{eff}(f)$ from directivity measurements for a membrane hydrophone [90] (*i.e.*, a non-RP system where sensitivity and directional responses may be significantly affected by internal waves within the sensing element). Benefits of using equivalent RB models to describe RP systems include 1) the RB model is easier and faster to compute, 2) the RB model offers a simpler, more intuitive formula for spatial averaging effects, and 3) the method recommended in IEC 62127-3 Section 5.6 for determination of hydrophone effective radius is based on the RB model [68]. The cost of using equivalent RB models to describe RP systems is that the less realistic model can lead to loss of accuracy, which will be investigated and quantified in the present paper.

The curve-fitting approach for determining $a_{eff}(f)$ was preferable for the present application to the approach recommended in IEC 62127-3 Section 5.6, which gives formulas for effective radius based on measurements of −3 dB and − 6 dB angles for directivities. The preference is because for low values of $ka_g$, RP directivities might not fall below −6 dB or even −3 dB within the range of angles investigated even if these angles go up to 90° (see Fig. 1 in [53] and Fig. 2 in [54]). The curve-fitting approach provides values for $a_{eff}(f)$ over a wider range of $ka_g$ than the IEC 62127-3 approach.

In principle, optimal model parameters derived from the fitting procedure could depend on the range of angles of plane wave propagation included in the fits. Ideally, the range of angles in the model fits should match the range of angles in the angular spectrum of the beam. In order to investigate the dependence of model parameters on angle range, model fits were performed for multiple angle ranges: ±10° ±20°, ±30°, … ±90°. The range of ±90° is appropriate for hemispherical arrays used in transcranial applications.

### C. KZK Simulation Methods

Simulations were performed to test for when a power law, $\sigma_n = \sigma_1 / n^q$, is appropriate to model the dependence of harmonic beam width on harmonic number and to estimate the value of the exponent $q$ as a function of experimental parameters. Simulations utilized HIFU Simulator software [91] available at the MathWorks web site. HIFU Simulator solves the KZK equation, which is the quadratic approximation of the Westervelt equation (not to be confused with the quadratic spatial averaging model discussed previously). The KZK equation is theoretically valid up to angles of about 15-20° from the propagation axis (roughly equivalent to F# > 1.5) [86, 92]. However, it has been reported that the KZK equation can be relatively accurate in the frequency domain about 25° from the transducer axis (F# = 1) [92]. The parameters for water used in the simulations were sound speed $c$ = 1480 m/s, density $\rho$ = 1 g/cm$^3$, absorption at 1 MHz = 0.217 dB/m, exponent of absorption vs. frequency curve = 2, and nonlinear coefficient $\beta$ = 3.5 (where the nonlinear coefficient $\beta$ should not be confused with the variable $\beta$ from section II.F). One hundred harmonics were used in each simulation.

Table II lists sets of transducer parameters used in simulations. One set of parameters corresponded to the Sonic Concepts H196, which is designed for HITU applications. Three sets of parameters corresponded to the transducers made by Blatek (State College, PA) and Panametrics (Waltham, MA) that were used in the experiments (see next section). Each simulation was repeated for a range of input powers in order to generate non-linear propagation parameter $\sigma_m$ [93] and local distortion parameter $\sigma_q$ [94] values for the focal point waveforms up to 5 and 6 respectively. Note that $\sigma_m$ is approximately equal to the local distortion parameter $\sigma_q$ when the local area factor $F_a$ (square root of the ratio of the source aperture area to beam area) is between 2 and 12 [94, 95]. The range of $\sigma_m$ and $\sigma_q$ investigated corresponded to spectral index $SI$ values ranging from 0.01 to 0.54. $SI$ is the fraction of the power spectrum contained in frequencies above the fundamental frequency [96, 97].

### D. Experimental Methods

Experiments were conducted to test the suitability of extending Blackstock's relative spectral weights from plane to focused waves, to test the Gaussian beam approximation, and to measure the exponent $q$ where $\sigma_n = \sigma_1 / n^q$. Table II lists the transducers used.

A Tektronix (Beaverton, OR) AFG 3102 function generator was used to generate tone bursts containing 6-10 cycles of the driving frequency. Each source transducer was driven at its center frequency and perhaps one or two additional frequencies off resonance to expand the parameter space for the measurements. The output of the function generator was connected to an Amplifier Research (Souderton, PA) 150A 100B 150 Watt power amplifier. The output of the power amplifier was connected to the source transducer. The ultrasound signal was received using an Onda (Sunnyvale, CA) GL-0085 capsule hydrophone with a nominal geometric sensitive element diameter of 85 μm. The hydrophone signal was digitized using a Tektronix TDS 3012 digital phosphor oscilloscope. The digitization rate was 1 GHz.

Axial hydrophone measurements at the geometrical focal point based on transducer surface curvature were used to test the suitability of using harmonic strengths with relative magnitudes computed from Blackstock's theory (which was derived for plane waves) to model focused beams. Spectra were obtained from Fast Fourier Transforms (FFTs) of axial hydrophone voltage signals. Complete, rectangular-windowed tone bursts (rather than windowed intervals from the middle) were analyzed. Spectra were deconvolved for sensitivity using the frequency-dependent sensitivity for the GL-0085. Blackstock's $\sigma$ (not to be confused with the Gaussian beam width parameter $\sigma_n$) was estimated by finding the set of coefficients $B_n(\sigma)$ from (7) with the minimum mean squared difference with the magnitudes of the experimental harmonics (maxima of spectral peaks near integer multiples of the fundamental frequency) in the FFT. Both $B_n(\sigma)$ and the experimental harmonic strengths were normalized to the magnitude for the fundamental spectral peak. Model spectra, which were constrained to be consistent with Blackstock's theory, were obtained by multiplying experimental spectra by the ratio of $B_n(\sigma)$ to the experimental harmonic spectra in the vicinities of each of the first 4-5 harmonics. Inverse FFTs were applied to model spectra to obtain model time-domain waveforms. Model time-domain waveforms were compared to measured waveforms.

Lateral hydrophone scans in the focal plane were used to 1) test the suitability of the Gaussian beam approximation and 2) measure the exponent $q$ where $\sigma_n = \sigma_1 / n^q$. Three lateral scans were performed for each combination of source transducer and driving frequency. The hydrophone was laterally scanned in spatial increments of 0.05 (Panametrics) – 0.06 (Blatek) mm. Lateral hydrophone scan data were Fast Fourier transformed to generate lateral beam plots for 4-5 harmonics. As before, complete tone bursts (rather than windowed intervals from the middle) were analyzed. Again, harmonic magnitudes were computed from maxima of spectral peaks near integer multiples of the fundamental frequency. The exponent $q$ was estimated by fitting HWHM to a power law proportional to $1 / n^q$. Similar methodology was reported by Ward *et al.* [88]. HWHM were measured by linear interpolation between the two lateral shifts corresponding to harmonic beam magnitude values just above and just below half the maximum (zero lateral shift) value.

## IV. Results

### A. Approximation of Rigid Piston Transfer Function with Rigid Baffle Transfer Function based on Frequency-Dependent Effective Sensitive Element Size.

Fig. 4 shows a scatter plot of $ka_{eff}$ vs. $ka_g$ where $a_{eff}$ is the value of $a$ in the RB directivity (5) that minimizes the mean square difference between RB model (for $a = a_{\text{eff}}$) and RP model (for $a_1 = a_2 = a_g$) directivities (over the range from $-60° < \theta < 60°$). It appears that $ka_{eff}$ exhibits the same dependence on $ka_g$ for all frequencies investigated. This is expected because the RP model is a purely geometrical model and therefore the response should only depend on the relative sizes of diameter and wavelength as described by the $ka_g$ values. For $ka_g > 4$, $ka_{eff}$ is approximately equal to $ka_g$. This is consistent with previous measurements of directivity for needle [53] and fiber optic [54] hydrophones. For $ka_g < 4$, $ka_{eff}$ tends to be greater than $ka_g$. At $ka_g = 0.5$, $ka_{eff} \approx 2.25\ ka_g$. At $ka_g = 1$, $ka_{eff} \approx 1.75\ ka_g$.

Fig. 5 shows the relative difference between $a_{eff}$ and $a_g$ as a function of $ka_g$ obtained with fits over the range of $-60° < \theta < 60°$. The decline of $a_{eff}$ with frequency is qualitatively consistent with reported measurements for needle [45, 53, 98] and fiber optic [54, 98] hydrophones. (Recall that $k = 2\pi f/c$.) Table III shows results of parametric fits for $(a_{eff} - a_g)/a_g$ for various angle ranges. The exponential fit has two parameters (A and B) and fits the data more closely than the single parameter inverse law fit. Exponential fits have also been found to be appropriate for experimental data from membrane hydrophones [90]. Parameters exhibit gradual dependences on angle range. Estimates for the numerator ($C$) values for the fit of the form $C/ka_g$ may be compared with previous reported measurements. (The numerator $C$ should not be confused with the correction factor $C$ defined in Section II.F. In both cases, the variable $C$ was chosen in order to be consistent with previous publications [38, 53, 54]). Wear *et al.* estimated $C$ using fits over the range of $-70° < \theta < 70°$ for four needle hydrophones with nominal geometric sensitive element diameters of 200, 400, 600, and 1000 μm. Their value of 0.52 (95% CI: 0.45 – 0.59) [53] is close to the value in Table III over the same angle range: 0.51 (95% CI: 0.46 – 0.56). Wear and Howard estimated $C$ using fits over the range of $-90° < \theta < 90°$ for a reflectance-based fiber optic hydrophone with nominal geometric sensitive element diameter of 105 μm. Their value of 0.67 (95% CI: 0.55 – 0.79) [54] is close to the value in Table III over the same angle range: 0.57 (95% CI: 0.52 – 0.62).

Fig. 6 shows magnitude and phase of directivity functions for four values of $ka_g$ for the RP model evaluated for $a_1 = a_2 = a_g$ and two versions of the RB model evaluated for $a = a_g$ and $a_{eff}(f)$. The top row of Fig. 6 illustrates that the directivity magnitude predicted by the RP model can be closely approximated by the directivity magnitude predicted by the RB model provided the effective sensitive element radius, $a_{eff}(f)$, is used. The bottom row of Figure 6 shows that the phase differences between the two models tend to be small, except sometimes near nulls in the directivity pattern. Since incident plane waves near angles corresponding to nulls are highly suppressed anyway, discrepancies in phase shifts between RP and RB models near nulls are unimportant.

Fig. 7 shows differences in magnitude and phase between the RP model directivity evaluated for $a_1 = a_2 = a_g$ and RB model directivity evaluated for $a = a_{eff}(f)$. Phase differences as functions of angle were weighted by directivity magnitude as a function of angle before averaging. The magnitude difference reaches a maximum of less than 3% near $ka_g = 5$. Fig. 7 suggests that the RP model evaluated for $a_1 = a_2 = a_g$ can be replaced by the RB model evaluated for $a = a_{eff}(f)$ for modeling spatial averaging effects of needle and reflectance-based fiber-optic hydrophones for many practical situations. This is convenient because the RB response can be easily and quickly computed by averaging the free field in space domain over the effective sensitive element area. This is easier than the implementing the RP directivity, which requires transformation to the spatial frequency domain and numerical computation of an integral.

## B. KZK Simulations

Fig. 8 shows simulation results for FWHM as functions of harmonic number for 6 transducers (see Table II) and a range of values for the nonlinear propagation parameter $\sigma_m$

[93]. The data presented include all harmonics for which harmonic power is at least six hundredths of one percent of the fundamental power. For $\sigma_m < 2.4$, $\sigma_m$ was highly correlated with the spectral index $SI$ [96], with the approximate formula $\sigma_m \approx 5.9\ SI$ achieving an RMSD of 0.1 compared with direct computation of $\sigma_m$. This approximate factor of 6 is similar to that found by Duck for a pulsed single element 3.38 MHz transducer with a focal depth of 95 mm (see Fig. 7 in [96]) and Duncan *et al.* for many transducers when energy transferred from the fundamental frequency to higher harmonics was less than 20 percent (see Fig. 5 in [94]).

For $\sigma_m < 2.4$ (which corresponds approximately and conservatively to $\sigma_q < 3$: $SI < 0.4$), the functions appear as straight lines on the log-log plots, indicating approximate power law relationships. For $\sigma_m > 2.4$ ($\sigma_q > 3$; $SI > 0.4$), the functions lose the straight-line appearance, indicating deviations from power laws. This suggests that the power law dependence of beam width on harmonic number is valid for $\sigma_m$ up to 2.4 and $\sigma_q$ up to 3 for the six transducers investigated. For $\sigma_m > 2.4$ ($\sigma_q > 3$; $SI > 0.4$), the beam widths for high harmonics are greater than would be predicted from a power law extension of low harmonic behavior (resulting in less spatial averaging), implying that a power-law model based on low harmonic behavior would yield an upper bound for spatial averaging reduction (*i.e.*, a lower bound for the spatial averaging filter), which may be useful for some applications.

Fig. 8 shows a slight upward trend for the fundamental FWHM (y-intercept) with $\sigma_m$. This might be attributable to loss of energy (that is, conversion to higher harmonics) from the center of the beam (where pressure is most intense) increasing with nonlinearity as discussed previously [83]. However, for all six transducers in Fig. 8 and all $\sigma_m$ values ranging from 0.02 to 5, the fundamental beam width remained within 6% of its theoretical value from (12), indicating that beam broadening was a small effect. This suggests that CJF conditions were valid for $\sigma_m$ up to 5 ($\sigma_q$ up to 6) for the transducers investigated in tone burst mode.

Fig. 9 shows simulation and experimental results for the dependence of the exponent $q$ of FWHM vs. harmonic number (based on a power law fit of the first 5 harmonics) on $\sigma_m$. For $\sigma_m < 5$ ($\sigma_q < 6$), $q$ mostly falls in the range between 0.6 and 0.8. A least-squares linear fit to the data (red line) is given by $q = 0.79 - 0.042\ \sigma_m$ (which corresponds to $q = 0.78 - 0.32\ \sigma_q$).

## C. Experimental Results to Test Assumptions Underlying Theoretical Framework

Fig. 9 shows that the experimental values for $q$ were consistent with simulated values (based on the first 5 harmonics), considering the range of $\sigma_m$. This supports the idea that measured harmonics were due to nonlinear propagation rather than by spurious harmonics generated at the transducer surface. (The presence of harmonics generated at the transducer surface would drive $q$ upward toward a value of 1 because their focused beam widths would be simply inversely proportional to frequency [81]). The nonlinearity metrics were $\sigma_m < 0.7$, $\sigma_q < 0.9$, and $SI < 0.1$. Nonlinearity was high enough to ensure multiple detectable harmonics but low enough to prevent 1) damage to hydrophones and 2) compromised measurements due to cavitation.

Fig. 10a shows a spectrum of a hydrophone measurement at the focus of the Blatek 3.5 MHz transducer. Relative harmonic magnitudes $B_n(\sigma)$ from Blackstock's theory (7) (red x's based on $\sigma$=0.35 and normalized to the fundamental magnitude) are consistent with measurements. Fig. 10b shows the corresponding time-domain radio-frequency (RF) signals. The measurement is shown in the blue line. A best-fit signal with relative harmonic strengths corresponding to Blackstock's theory (7) with $\sigma$=0.35 is shown in the red dashed line. The RMSD between experimental and best-fit theoretical harmonic coefficients was 16% ± 1% for three transducers (Blatek and two Panametrics transducers in Table II). Therefore, although Blackstock's spectral coefficients were derived for plane waves, they appear to provide reasonable spectral weights to model focused beams considered in this study.

Fig. 11 shows lateral beam scans for harmonics for the Blateck 3.5 MHz transducer. The solid black line shows the theoretical CJF radial profile at the fundamental frequency. The dotted black line shows a Gaussian fit to the lateral profile at the fundamental frequency. The dotted lines for the harmonics were generated by reducing the width parameter for the fundamental radial profile by a factor of $1 / n^q$, where $q$ was obtained by fitting HWHM($n$) to a power law proportional to $1 / n^q$. The RMSD between experimental HWHM and functional fits was 0.0097 ± 0.0049 mm (4.0 ± 1.9%) for the first 4 harmonics over all 5 transducer / frequency combinations. The data support the Gaussian form for the fundamental and harmonic components of the beam. Estimates for the exponent $q$ were approximately 0.8 as shown in Table II. This is larger than the quasilinear value of 0.5 [76, 78] and the experimental value of 0.61 reported by Ward *et al.* [88], but consistent with KZK simulations (see Fig. 9).

### D. Simulation Examples of Hydrophone Transfer Functions and Their Effects on Signals

Fig. 12 shows simulated RP ($a_1$=$a_2$=$a_g$) and RB ($a$= $a_{eff}(f)$) transfer functions, $H_{RP}(f)$ and $H_{RB}(f)$, for the case of a Sonic Concepts H101 transducer operated at its lower frequency mode of 1.05 MHz (under CJF conditions) for $q$ = 0.8. The simulated hydrophone sensitive element geometrical diameter was 200 μm. $H_{RP}(f)$ and $H_{RB}(f)$ are essentially identical, which supports the separable model and the expedient usage of the RB transfer function, provided $a_{eff}(f)$ is used rather than $a_g$. As frequency increases from 0, $H_{RP}(f)$ and $H_{RB}(f)$ increase until $f$ reaches $f_{max} = 1.2c / (\pi a_g)$ = 5.7 MHz. Beyond $f_{max}$, the hydrophone sensitivity $M_L(f)$ is relatively flat and therefore $H_{RP}(f)$ and $H_{RB}(f)$ decrease due to spatial averaging effects. Fig. 12 also shows the spatial averaging filter for the RP model, $S_{RP}(f) = H_{RP}(f) / M_L(f)$, which is very consistent with 1) the integral form computed from the pressure wave model combined with the numerical RP model (17) and 2) the analytic (Gaussian) formula for $S_p(f)$ (20). Since the numerical integral form (17) accounts for phase of the diffraction pattern and the analytic (Gaussian) form (20) neglects phase of the diffraction pattern, their similarity suggests that phase of the diffraction pattern may be safely neglected when predicting spatial averaging effects. The quadratic form for $S_p(f)$ given by (30), a harmonic extension of IEC 627127-1 Annex E, is valid up to about $n$ = 19 as predicted by (33), corresponding to $f$ = 20 MHz as shown in the black vertical chain-dash line.

Fig. 13 shows the effects of $H_{RP}(f)$ and $H_{RB}(f)$ from Fig. 12 on a tone burst. The time domain effects of $H_{RP}(f)$ and $H_{RB}(f)$ are essentially identical, which again supports the separable model and the expedient usage of the RB transfer function, provided $a_{eff}(f)$ is used rather than $a_g$. All harmonic frequencies up to about 25 MHz are boosted relative to the fundamental (see $H_{RP}$ and $H_{RB}$ in Fig. 12). Since most of the energy in the signal spectrum lies mostly below 25 MHz, this results in high-pass filtering, producing higher, sharper compressional peaks than in the undistorted case.

Fig. 14 shows simulated RP ($a_1=a_2=a_g$) and RB ($a= a_{eff}(f)$) transfer functions, $H_{RP}(f)$ and $H_{RB}(f)$, for the case of a Sonic Concepts H101 transducer operated at its higher frequency mode of 3.3 MHz (under CJF conditions) for $q = 0.8$. Again, the simulated hydrophone geometrical sensitive element diameter was 200 μm. $H_{RP}(f)$ and $H_{RB}(f)$ are essentially identical, which supports the expedient usage of the RB transfer function, provided $a_{eff}(f)$ is used rather titan $a_g$. At 3.3 MHz, unlike 1.05 MHz, the high-pass filter effect of $M_L(f)$ at low frequencies is not very apparent because the fundamental frequency is relatively close (within a factor of 2) to $f_{max} = 1.2c / (\pi a_g) = 5.7$ MHz. Therefore, Fig. 14 mostly shows the effects of spatial averaging. Fig. 14 also shows the spatial averaging filter for the RP model, $S_{RP}(f) = H_{RP}(f) / M_L(f)$, which is very consistent with 1) the integral form computed from the pressure wave model combined with the numerical RP model (17) and 2) the analytic (Gaussian) form for $S_p(f)$ (20). Since the numerical integral form (17) accounts for phase of the diffraction pattern and the analytic (Gaussian) form (20) neglects phase of the diffraction pattern, their similarity suggests that phase of the diffraction pattern may be safely neglected when predicting spatial averaging effects. The quadratic form for $S(f)$ given by (30) is valid up to about $n = 4$ as predicted by (33), corresponding to $f = 13$ MHz as shown in the black vertical chain-dash line.

Fig. 15 shows the effects of $H_{RP}(f)$ and $H_{RB}(f)$ from Fig. 14 on a tone burst. The time domain effects of $H_{RP}(f)$ and $H_{RB}(f)$ are essentially identical, which again supports the expedient usage of the RB transfer function, provided $a_{eff}(f)$ is used rather than $a_g$. At 1.05 MHz, high-pass filter effects dominate spatial averaging effects, leading to higher, sharper compressional peaks (Fig. 13). In contrast, at 3.3 MHz, spatial averaging effects dominate high-pass filter effects, leading to smaller, rounded compressional peaks (Fig. 15).

## V. Graphical Guide

Fig.s 16 – 18 show the Graphical Guide for visualizing the effect of F# and ratio of geometrical sensitive element diameter to fundamental wavelength on hydrophone sensitivity (“M”, blue circles) and spatial averaging filter (“S”, red squares) for the CJF model. The total spatiotemporal transfer function is the product of M and S. Sensitivities in the Graphical Guide have been normalized so that their values at the first harmonic are equal to one. The spatial averaging filter was computed for $q = 0.2$, 0.4, 0.6, and 0.8 where the full width half maxima of harmonic beams are proportional to the FWHM of the fundamental beam divided by $n^q$ where $n$ is the harmonic number. For nonlinear propagation parameter $\sigma_m < 2.4$ ($\sigma_q < 3$) or spectral index $SI < 0.4$ (that is, less than 40% of signal power contained harmonics above the fundamental), $q$=0.81-0.38$SI$ for the six transducers investigated here (see Table II) so that $q$ mostly ranges from 0.6 to 0.8 (see Fig. 9). (See next section for

further discussion of values for $q$ in quasi-linear applications.) For $\sigma_m > 2.4$ ($\sigma_q > 3$: $SI > 0.4$), the relation between FWHM and $n$ deviates from a power law and effective values for $q$ would be expected to decrease below 0.6, as may be seen from the slopes (*i.e.*, power law exponents) of the curves in Fig. 8. (Note that the values for $q$ in Fig. 9 are based only on the first 5 harmonics and would be lower if based on all significant harmonics for $\sigma_m > 2.4$ or $\sigma_q > 3$.)

In order to maximize the utility of the Graphical Guide, an investigator should have some idea of the effective number of harmonics in the signal to be measured. Then the investigator can look at the plots in the Graphical Guide over the effective range of harmonics to determine whether a sensitivity deconvolution or a spatial averaging correction or both would be required. If the sensitivity M varies considerably over the effective range of harmonics, then a sensitivity deconvolution would be advisable. If the spatial averaging filter S decreases substantially below one over the effective range of harmonics, then a spatial averaging correction would be advisable.

(Note that a sensitivity deconvolution might also be advisable even for linear signals if the hydrophone sensitivity is not sufficiently uniform over the band of frequencies in the signal [89].)

While the RP model has been demonstrated to accurately represent needle sensitivity at low frequencies, experimentally measured sensitivity can deviate from the RP model at frequencies above $2f_{max}$, where $f_{max} = 1.2c / (\pi a)$ [52]. This is likely due to design complexities in real needle hydrophones that are not captured by the RP model such as thickness-mode resonances of the sensing element and limited bandwidth due to amplifier electronics. The frequency range for validity for fiber optic hydrophones appears to be greater than that for needle hydrophones (see Fig. 10 in [52]). In actual practice, it is probably advisable to deconvolve with experimentally-measured sensitivity if available rather than theoretical model sensitivity. However, this may not be possible in the planning stages of an experiment, before a hydrophone has been acquired. The Graphical Guide gives reasonable projections for many RP hydrophone sensitivities for frequencies at least up to $2f_{max}$.

## VI. Discussion

Most investigations of hydrophone signal distortion have considered frequency-dependent sensitivity [14, 30-36] or spatial averaging [37-41, 43, 44, 46-48] but not both. The present paper combines both sources of distortion in a model appropriate for hydrophones that can be accurately modeled as rigid pistons, including needle and reflectance-based fiber optic hydrophones. The model demonstrates conditions under which the hydrophone transfer function may be represented as separable in cylindrical coordinates. Separability provides convenience in that the two deconvolutions can be applied independently. The model allows deconvolution for beams in which the fundamental and harmonic radial pressure distributions may be approximated as Gaussians (at least within the spatial extent the hydrophone sensitive element), provided that the harmonic-dependent beam width is known. In the special case of a classic-jinc-fundamental (CJF) beam, the formulas for beam widths

may be simplified. When the harmonic-dependent beam width can be approximated as decreasing as $n^q$ (which was verified for $\sigma_m$ up to 2.4, $\sigma_q$ up to 3, and *SI* up to forty percent for a variety of transducer geometries), additional simplification is possible.

The method for correction for spatial averaging provided in the present paper applies to all types of hydrophones with circular symmetry, not just needle and fiber optic hydrophones. The method offers some advantages over the method prescribed in IEC 62127-1 Annex E, which is based on the seminal work by Preston *et al.* [38]: 1) It offers an analytic expression for the spatial averaging filter (the reciprocal of the spatial averaging correction factor) in terms of beam and hydrophone dimensions. 2) It does not require an additional measurement at one hydrophone radius from the axis. Such a measurement creates an extra experimental burden and there may be error if the hydrophone off-axis displacement differs from exactly one hydrophone radius. (Note that IEC 62127-1 specifies that this displacement should be equal to the *effective* hydrophone radius, which is frequency-dependent and not as accessible as the *geometrical* hydrophone radius.) Also, such a measurement may not always be available, especially when data are analyzed retrospectively. 3) It accommodates nonlinear signals that contain many harmonics, as are commonly encountered today in therapeutic and Doppler applications. To be fair, Preston *et al.* could not have been expected to foresee the substantial rise of nonlinear ultrasound that has occurred since 1988, when their pioneering paper was published. Preston's formula was adequate for most situations that were encountered at the time. 4) In combination with the formula that relates effective hydrophone radius to geometrical hydrophone radius, the spatial averaging filter obtained in the present paper can be used to predict spatial averaging in terms of the easily accessible geometrical hydrophone radius rather than the less accessible frequency-dependent effective hydrophone radius, which is often estimated from directivity measurements (as recommended in IEC 62127-3 Section 5.6). 5) It does not assume a quadratic radial pressure distribution that limits applicability roughly to within the full width half maximum (FWHM) of the beam. This feature allows greater application to high frequency fields, whether generated by a high fundamental frequency or harmonics of a low fundamental frequency (in the case of HITU). Finally, although the spatial averaging correction in the present paper assumes Gaussian harmonic beams (within the spatial extent of the hydrophone sensitive element), this approximation should not be more objectionable than Preston *et al.*'s assumption of quadratic beams (as may be seen in Fig. 3).

An important variable in determining spatial averaging effects is the exponent $q$ that gives the power law dependence of beam width with harmonic number, $\sigma_n = \sigma_1 / n^q$. It is instructive to compare the values of $q$ measured in the present paper with values reported from previous studies. In the present study, $q$ ranged from 0.76 – 0.84, consistent with predictions using the KZK equation as shown in Fig. 9. O'Reilly and Parker measured beam widths that varied approximately as $1/\sqrt{n}$ ($q = 0.5$) for the fundamental through fifth harmonic ($f_1$ = 1.75-3.38 MHz, $a_s$ = 12.7 mm, $D$ = 80 mm) [99]. Ward *et al.* measured $q$ = 0.61 from 4 harmonics ($f_1$ = 2.25 MHz, $a_s$ = 19 mm, $D$ = 262 mm) [88]. Cherin *et al.* reported measurements of beam widths for the fundamental at 20 MHz (136.9 ± 1.4 μm) and a harmonic at 40 MHz (77.3 ± 2.0 μm) ($f_1$ = 20 MHz, $a_s$ = 3 mm, $D$ = 10 mm). Based on these two values, their beam widths were consistent with $q$ = 0.82. Although Averkiou and

Hamilton made similar measurements of harmonic radial beam patterns, they presented their results graphically but not numerically, precluding an accurate estimate of $q$ [80]. One source for disparity in values for $q$ is that, as Fig. 9 shows, $q$ depends on $\sigma_m$. Another source of disparity is hydrophone technology used to measure harmonic beam widths. The measurements of harmonic beam widths required for the estimation of $q$ in the present paper may have benefitted from higher resolution hydrophone measurements than were possible with the hydrophone technology available when some of earlier papers were published. Hydrophone sensitive element diameters were 85 μm (present paper), 1mm [99], 1 mm [88], and 25 μm [100].

While the present paper together with its sequel [75] investigated (analytically, numerically, and experimentally) hydrophone spatial averaging of nonlinear tone bursts, Cooling *et al.* investigated (numerically) spatial averaging of nonlinear waveforms containing just a few cycles [46], which can be important in the context of hydrophone calibration [30, 90, 101]. While the present paper computed spatial averaging filters only at harmonic frequencies (where most of the tone burst signal energy is). Cooling *et al.* obtained quasi-continuous spatial averaging filters. Therefore, the present paper is particularly relevant to tone burst signals such as those used in diagnostic Doppler mode, HITU, and quasi-continuous-wave applications. (The effects of RP sensitivity on broadband signals are considered in [52].) Spatial averaging filters at harmonic frequencies in both papers were low-pass filters that decrease monotonically from 1 to 0 as frequency increases from 0 to infinity. Radulescu *et al.* investigated numerically-computed spatial averaging filters for linear signals in the context of correcting hydrophone calibrations [47] and also found monotonic, low-pass, spatial averaging filters. The present paper, unlike the other two, derived an analytic expression for the spatial averaging filter. The model incorporated a validated theoretical model (RP model) for needle and fiber optic hydrophones to derive frequency-dependent effective sensitive element size.

Some limitations of this paper are as follows. First, if the source is a circular focused piston transducer (the most common source geometry), the separability and Gaussian beam assumptions may limit the model to near the focal region. (For example, Averkiou and Hamilton showed quasi-Gaussian behavior for propagation distances between 75% and 156% of the focal distance for an F/4.25 transducer [80].) It should be noted, however, that the focal region is where the beam is most intense and pressure measurement is most critical. Second, while the RP model has been demonstrated to accurately represent needle sensitivity at low frequencies, experimentally measured sensitivity can deviate from the RP model at frequencies above $2f_{max}$ where $f_{max} = 1.2c / (\pi a)$ [52], especially for needle hydrophones, due to design complexities not captured by the RP model. Third, while the general Gaussian (GG) form of the model allows for distortion of the classic-jinc-fundamental (CJF) form for the fundamental radial pressure distribution, it requires knowledge of the harmonic-dependent beam widths, which can be difficult to ascertain. On the other hand, the CJF version of the model requires minimal distortion of the fundamental radial pressure distribution. However, Fig. 8 shows little change in FWHM (y-intercept value) with $\sigma_m$ and therefore suggests that this assumption is valid for circular focused piston transducers for $\sigma_m$ up to 5, and therefore applicable to a wide variety of nonlinear ultrasound beams. Fourth, the CJF form of the theory is valid for F#s of approximately one

and above. HIFU transducers can have lower F#s. The experimental validation and KZK simulations were limited to transducers with F#s between 1.4 and 2.5.

## VII. Conclusion

The spatiotemporal transfer function for a needle or reflectance-based fiber-optic hydrophone was modeled as separable into the product of two filters corresponding to frequency-dependent sensitivity and spatial averaging. The separable hydrophone transfer function model was verified by comparison to a more general rigid piston spatiotemporal response model that did not assume separability. An analytic formula for a spatial averaging correction that applies to all hydrophones (not just needle and fiber optic hydrophones) was derived. Simulation analysis indicated that the spatial averaging correction is valid for highly nonlinear signals. The spatial averaging correction recommended by IEC 62127-1, Annex E, was extended to nonlinear signals with multiple harmonics. A graphical guide was presented to help investigators choose and defend appropriate hydrophone sensitive element size for their measurements of ultrasound signals.

## Acknowledgements

The mention of commercial products, their sources, or their use in connection with material reported herein is not to be construed as either an actual or implied endorsement of such products by the Department of Health and Human Services. The authors are grateful for funding support from the FDA Office of Women's Health. The author is grateful to Gerald R. Harris for providing him with an excellent education on hydrophones.

## Biography

**Keith A. Wear** received his B.A. in Applied Physics from the University of California at San Diego. He received his M.S. and Ph.D. in Applied Physics with a Ph.D. minor in Electrical Engineering from Stanford University. He was a post-doctoral research fellow with the Physics department at Washington University, St. Louis. He is the FDA Acoustics Laboratory Leader. He is an Associate Editor of 3 journals: *Journal of the Acoustical Society of America, IEEE Transactions on Ultrasonics, Ferroelectrics, and Frequency Control*; and *Ultrasonic Imaging*. He was the Technical Program Chair of the 2008 IEEE International Ultrasonics Symposium in Beijing, China. He was the General Program Chair of the 2017 IEEE International Ultrasonics Symposium in Washington, DC. He was chair of the American Institute of Ultrasound in Medicine (AIUM) Technical Standards Committee from 2014-2016. He is a Fellow of the Acoustical Society of America, the American Institute for Medical and Biological Engineering, and the AIUM. He is a senior member of IEEE.

## REFERENCES

[1]. Harris GR, "Hydrophone Measurements in Diagnostic Ultrasound Fields," IEEE Trans Ultrason Ferroelectr Freq Control, vol. 35, no. 2, pp. 87–101, 3 1988. [PubMed: 18290135]

[2]. Harris GR, "Progress in medical ultrasound exposimetry," IEEE Trans Ultrason Ferroelectr Freq Control, vol. 52, no. 5, pp. 717–36, 5 2005. [PubMed: 16048175]

[3]. Szabo TL, Diagnostic Ultrasound Imaging: Inside Out, Second ed. Oxford, UK: Elsevier, 2014.

[4]. Hynynen K et al., "500-element ultrasound phased array system for noninvasive focal surgery of the brain: a preliminary rabbit study with ex vivo human skulls," Magn Reson Med, vol. 52, no. 1, pp. 100–7, 7 2004. [PubMed: 15236372]

[5]. Clement GT, "Spectral image reconstruction for transcranial ultrasound measurement," Phys Med Biol, vol. 50, no. 23, pp. 5557–72, 12 07 2005. [PubMed: 16306652]

[6]. White J, Clement GT, and Hynynen K, "Transcranial ultrasound focus reconstruction with phase and amplitude correction," IEEE Trans Ultrason Ferroelectr Freq Control, vol. 52, no. 9, pp. 1518–22, 9 2005. [PubMed: 16285450]

[7]. Choi JJ, Pernot M, Small SA, and Konofagou EE, "Noninvasive, transcranial and localized opening of the blood-brain barrier using focused ultrasound in mice," Ultrasound Med Biol, vol. 33, no. 1, pp. 95–104, 1 2007. [PubMed: 17189051]

[8]. Konofagou EE, "Optimization of the ultrasound-induced blood-brain barrier opening," Theranostics, vol. 2, no. 12, pp. 1223–37, 2012. [PubMed: 23382778]

[9]. Konofagou EE, Tung YS, Choi J, Deffieux T, Baseri B, and Vlachos F, "Ultrasound-induced blood-brain barrier opening," Curr Pharm Biotechnol, vol. 13, no. 7, pp. 1332–45, 6 2012. [PubMed: 22201586]

[10]. Robertson J, Martin E, Cox B, and Treeby BE, "Sensitivity of simulated transcranial ultrasound fields to acoustic medium property maps," Phys Med Biol, vol. 62, no. 7, pp. 2559–2580, 4 07 2017. [PubMed: 28165334]

[11]. Robertson JL, Cox BT, Jaros J, and Treeby BE, "Accurate simulation of transcranial ultrasound propagation for ultrasonic neuromodulation and stimulation," J Acoust Soc Am, vol. 141, no. 3, p. 1726, 3 2017. [PubMed: 28372121]

[12]. Zanelli CI and Howard SM, "A robust hydrophone for HIFU metrology," (in English), Therapeutic Ultrasound, vol. 829, pp. 618-+, 2006.

[13]. Haller J, Jenderka KV, Durando G, and Shaw A, "A comparative evaluation of three hydrophones and a numerical model in high intensity focused ultrasound fields," (in English), J. Acoust. Soc. Am, vol. 131, no. 2, pp. 1121–1130, 2 2012. [PubMed: 22352487]

[14]. Liu Y, Wear KA, and Harris GR, "Variation of High-Intensity Therapeutic Ultrasound (HITU) Pressure Field Characterization: Effects of Hydrophone Choice, Nonlinearity, Spatial Averaging and Complex Deconvolution," Ultrasound Med Biol, vol. 43, no. 10, pp. 2329–2342, 10 2017. [PubMed: 28735734]

[15]. Rahim A, Taylor SL, Bush NL, ter Haar GR, Bamber JC, and Porter CD, "Physical parameters affecting ultrasound/microbubble-mediated gene delivery efficiency in vitro," Ultrasound Med Biol, vol. 32, no. 8, pp. 1269–79, 8 2006. [PubMed: 16875960]

[16]. Brown JA, Foster FS, Needles A, Cherin E, and Lockwood GR, "Fabrication and performance of a 40-MHz linear array based on a 1-3 composite with geometric elevation focusing," IEEE Trans Ultrason Ferroelectr Freq Control, vol. 54, no. 9, pp. 1888–94, 9 2007. [PubMed: 17941395]

[17]. Holt RG and Roy RA, "Measurements of bubble-enhanced heating from focused, MHz-frequency ultrasound in a tissue-mimicking material," Ultrasound Med Biol, vol. 27, no. 10, pp. 1399–412, 10 2001. [PubMed: 11731053]

[18]. Giesecke T and Hynynen K, "Ultrasound-mediated cavitation thresholds of liquid perfluorocarbon droplets in vitro," Ultrasound Med Biol, vol. 29, no. 9, pp. 1359–65, 9 2003. [PubMed: 14553814]

[19]. Wear KA, Gammell PM, Maruvada S, Liu Y, and Harris GR, "Time-delay spectrometry measurement of magnitude and phase of hydrophone response," IEEE Trans Ultrason Ferroelectr Freq Control, vol. 58, no. 11, pp. 2325–33, 11 2011. [PubMed: 22083766]

[20]. Staudenraus J and Eisenmenger W, "Fiberoptic Probe Hydrophone for Ultrasonic and Shock-Wave Measurements in Water," (in English), Ultrasonics, vol. 31, no. 4, pp. 267–273, 7 1993.

[21]. Canney MS, Bailey MR, Crum LA, Khokhlova VA, and Sapozhnikov OA, "Acoustic characterization of high intensity focused ultrasound fields: A combined measurement and modeling approach," (in English), J. Acoust. Soc. Am, vol. 124, no. 4, pp. 2406–2420, 10 2008. [PubMed: 19062878]

[22]. Maxwell AD et al., "Cavitation clouds created by shock scattering from bubbles during histotripsy," (in English), J. Acoust. Soc. Am, vol. 130, no. 4, pp. 1888–1898, 10 2011. [PubMed: 21973343]

[23]. Kreider W et al., "Characterization of a Multi-Element Clinical HIFU System Using Acoustic Holography and Nonlinear Modeling," (in English), IEEE Trans Ultrason Ferroelectr Freq Control, vol. 60, no. 8, pp. 1683–1698, 8 2013. [PubMed: 25004539]

[24]. Lewin PA, Mu C, Umchid S, Daryoush A, and El-Sherif M, "Acousto-optic, point receiver hydrophone probe for operation up to 100 MHz," (in English), Ultrasonics, vol. 43, no. 10, pp. 815–821, 12 2005. [PubMed: 16054665]

[25]. Parsons JE, Cain CA, and Fowlkes JB, "Cost-effective assembly of a basic fiber-optic hydrophone for measurement of high-amplitude therapeutic ultrasound fields," (in English), J. Acoust. Soc. Am, vol. 119, no. 3, pp. 1432–1440, 3 2006. [PubMed: 16583887]

[26]. Umchid S et al., "Development of calibration techniques for ultrasonic hydrophone probes in the frequency range from 1 to 100 MHz," (in English), Ultrasonics, vol. 49, no. 3, pp. 306–311, 3 2009. [PubMed: 19110289]

[27]. Jing Y, Cannata J, and Wang T, "Experimental verification of transient nonlinear acoustical holography," J Acoust Soc Am, vol. 133, no. 5, pp. 2533–40, 5 2013. [PubMed: 23654362]

[28]. Vlaisavljevich E et al., "Effects of ultrasound frequency and tissue stiffness on the histotripsy intrinsic threshold for cavitation," Ultrasound Med Biol, vol. 41, no. 6, pp. 1651–67, 6 2015. [PubMed: 25766571]

[29]. Maxwell AD et al., "Fragmentation of urinary calculi in vitro by burst wave lithotripsy," J Urol, vol. 193, no. 1, pp. 338–44, 1 2015. [PubMed: 25111910]

[30]. Wilkens V and Koch C, "Amplitude and phase calibration of hydrophones up to 70 MHz using broadband pulse excitation and an optical reference hydrophone," (in English), J. Acoust. Soc. Am, vol. 115, no. 6, pp. 2892–2903, 6 2004.

[31]. Hurrell A, "Voltage to Pressure Conversion: Are you getting "phased" by the problem," (in English), AMUM 2004: Advanced Metrology for Ultrasound in Medicine 2004, vol. 1, pp. 57–62, 2004.

[32]. Wear KA, Gammell PM, Maruvada S, Liu Y, and Harris GR, "Improved measurement of acoustic output using complex deconvolution of hydrophone sensitivity," IEEE Trans Ultrason Ferroelectr Freq Control, vol. 61, no. 1, pp. 62–75, 1 2014. [PubMed: 24402896]

[33]. Wear KA, Liu YB, Gammell PM, Maruvada S, and Harris GR, "Correction for Frequency-Dependent Hydrophone Response to Nonlinear Pressure Waves Using Complex Deconvolution

and Rarefactional Filtering: Application With Fiber Optic Hydrophones," (in English), IEEE Trans. Ultrason. Ferroelectr. Freq. Control, vol. 62, no. 1, pp. 152–164, 1 2015. [PubMed: 25585399]

[34]. Eichstadt S and Wilkens V, "GUM2DFT-a software tool for uncertainty evaluation of transient signals in the frequency domain," (in English), Meas. Sci. Tech, vol. 27, no. 5, 5 2016.

[35]. Eichstadt S, Wilkens V, Dienstfrey A, Hale P, Hughes B, and Jarvis C, "On challenges in the uncertainty evaluation for time-dependent measurements," (in English), Metrologia, vol. 53, no. 4, pp. S125–S135, 8 2016.

[36]. Hurrell AM and Rajagopal S, "The Practicalities of Obtaining and Using Hydrophone Calibration Data to Derive Pressure Waveforms," (in English), IEEE Trans. Ultrason., Ferroelectr. Freq. Control, vol. 64, no. 1, pp. 126–140, 1 2017. [PubMed: 27479961]

[37]. Beissner K, "Maximum hydrophone size in ultrasonic field measurements," Acustica, vol. 59, pp. 61–66, 1985.

[38]. Preston RC, Bacon DR, and Smith RA, "Calibration of medical ultrasonic equipment-procedures and accuracy assessment," IEEE Trans Ultrason Ferroelectr Freq Control, vol. 35, no. 2, pp. 110–21, 1988. [PubMed: 18290137]

[39]. Smith RA, "Are hydrophones of diameter 0.5 mm small enough to characterise diagnostic ultrasound equipment?," Phys Med Biol, vol. 34, no. 11, pp. 1593–607, 11 1989. [PubMed: 2685834]

[40]. Zeqiri B and Bond AD, "The Influence of Wave-Form Distortion on Hydrophone Spatial-Averaging Corrections - Theory and Measurement," (in English), J. Acoust. Soc. Am, vol. 92, no. 4, pp. 1809–1821, 10 1992.

[41]. Boutkedjirt T and Reibold R, "Improvement of the lateral resolution of finite-size hydrophones by deconvolution," Ultrasonics, vol. 38, no. 1-8, pp. 745–8, 3 2000. [PubMed: 10829764]

[42]. Radulescu E, Lewin PA, Goldstein A, and Nowicki A, "Hydrophone spatial averaging corrections from 1-40 MHz," (in English), 2000 Ieee Ultrasonics Symposium Proceedings, *Vols* 1 and 2, pp. 1685–1688, 2000.

[43]. Boutkedjirt T and Reibold R, "Reconstruction of ultrasonic fields by deconvolving the hydrophone aperture effects. I. Theory and simulation," Ultrasonics, vol. 39, no. 9, pp. 631–9, 8 2002. [PubMed: 12206630]

[44]. Boutkedjirt T and Reibold R, "Reconstruction of ultrasonic fields by deconvolving the hydrophone aperture effects. II. Experiment," Ultrasonics, vol. 39, no. 9, pp. 641–8, 8 2002. [PubMed: 12206631]

[45]. Radulescu EG, Lewin PA, Nowicki A, and Berger WA, "Hydrophones' effective diameter measurements as a quasi-continuous function of frequency," (in English), Ultrasonics, vol. 41, no. 8, pp. 635–641, 11 2003. [PubMed: 14585475]

[46]. Cooling MP, Humphrey VF, and Wilkens V, "Hydrophone area-averaging correction factors in nonlinearly generated ultrasonic beams," J. Phys. Conf. Series, Adv. Metro for Ultrasound in Med, vol. 279, pp. 1–6, 2011.

[47]. Radulescu EG, Lewin PA, Goldstein A, and Nowicki A, "Hydrophone spatial averaging corrections from 1 to 40 MHz," (in English), IEEE Trans Ultrason Ferroelectr Freq Control, vol. 48, no. 6, pp. 1575–1580, 11 2001. [PubMed: 11800120]

[48]. Radulescu EG, Lewin PA, and Nowicki A, "1-60 MHz measurements in focused acoustic fields using spatial averaging corrections," Ultrasonics, vol. 40, no. 1-8, pp. 497–501, 5 2002. [PubMed: 12159990]

[49]. Jones DS, "The Scattering of a Scalar Wave by a Semi-Infinite Rod of Circular Cross Section," (in English), Philosophical Transactions of the Royal Society of London Series a-Mathematical and Physical Sciences, vol. 247, no. 934, pp. 499–528, 1955.

[50]. Krucker JF, Eisenberg A, Krix M, Lotsch R, Pessel M, and Trier HG, "Rigid piston approximation for computing the transfer function and angular response of a fiber-optic hydrophone," (in English), J. Acoust. Soc. Am, vol. 107, no. 4, pp. 1994–2003, 4 2000. [PubMed: 10790026]

[51]. Harris GR and Gammell PM, "Sensitivity measurements of piezoelectric polymer hydrophones from 0.2-2 MHz using a broadband-pulse technique," (in English), Journal of the Acoustical Society of America, vol. 105, no. 2, pp. 725–731, 2 1999.

[52]. Wear KA, Liu Y, and Harris GR, "Pressure pulse distortion by needle and fiber-optic hydrophones due to nonuniform sensitivity," IEEE Trans Ultrason Ferroelectr. Freq Control, vol. 65, no. 2, pp. 137–148, 2018. [PubMed: 29389648]

[53]. Wear KA, Baker C, and Miloro P, "Directivity and Frequency-Dependent Effective Sensitive Element Size of Needle Hydrophones: Predictions from Four Theoretical Forms Compared with Measurements," IEEE Trans Ultrason Ferroelectr Freq Control, vol. 65, no. 10, pp. 1781–1788, 2018. [PubMed: 30010557]

[54]. Wear KA and Howard SM, "Directivity and frequency-dependent effective sensitive element size of a reflectance-based fiber optic hydrophone: predictions from theoretical models compared with measurements," IEEE Trans Ultrason Ferroelectr Freq Control, no. in press, 2018.

[55]. Wang ZQ, Lauxmann P, Wurster C, Kohler M, Gompf B, and Eisenmenger W, "Impulse response of a fiber optic probe hydrophone determined with shock waves in water," (in English), J. Appl. Phys, vol. 85, no. 5, pp. 2514–2516, 3 1 1999.

[56]. Arvengas A, Davitt K, and Caupin F, "Fiber optic probe hydrophone for the study of acoustic cavitation in water," (in English), Rev Sci Instrum, vol. 82, no. 3, 3 2011.

[57]. Howard SM, "Calibration of Reflectance-Based Fiber-Optic Hydrophones," (in English), 2016 IEEE Intl. Ultrasonics Symp, 2016.

[58]. Haller J, Wilkens V, Jenderka KV, and Koch C, "Characterization of a fiber-optic displacement sensor for measurements in high-intensity focused ultrasound fields," (in English), J. Acoust. Soc. Am, vol. 129, no. 6, pp. 3676–3681, 6 2011. [PubMed: 21682392]

[59]. Weise W, Wilkens V, and Koch C, "Frequency response of fiber-optic multilayer hydrophones: Experimental investigation and finite element simulation," (in English), IEEE Trans. Ultrason. Ferroelectr. Freq. Control, vol. 49, no. 7, pp. 937–946, 7 2002. [PubMed: 12152948]

[60]. Cox BT, Zhang EZ, Laufer JG, and Beard PC, "Fabry Perot polymer film fibre-optic hydrophones and arrays for ultrasound field characterisation," (in English), AMUM 2004: Advanced Metrology for Ultrasound in Medicine 2004, vol. 1, pp. 32–37, 2004.

[61]. Morris P, Hurrell A, Shaw A, Zhang E, and Beard P, "A Fabry-Perot fiber-optic ultrasonic hydrophone for the simultaneous measurement of temperature and acoustic pressure," (in English), J. Acoust. Soc. Am, vol. 125, no. 6, pp. 3611–3622, 6 2009. [PubMed: 19507943]

[62]. Kim KS, Mizuno Y, and Nakamura K, "Fiber-optic ultrasonic hydrophone using short Fabry-Perot cavity with multilayer reflectors deposited on small stub," (in English), Ultrasonics, vol. 54, no. 4, pp. 1047–1051, 4 2014. [PubMed: 24411816]

[63]. Martin E, Zhang EZ, Guggenheim JA, Beard PC, and Treeby BE, "Rapid Spatial Mapping of Focused Ultrasound Fields Using a Planar Fabry-Perot Sensor," IEEE Trans Ultrason Ferroelectr Freq Control, vol. 64, no. 11, pp. 1711–1722, 11 2017. [PubMed: 28880170]

[64]. Vannacci E, Granchi S, Belsito L, Roncaglia A, and Biagi E, "Wide bandwidth fiber-optic ultrasound probe in MOMS technology: Preliminary signal processing results," (in English), Ultrasonics, vol. 75, pp. 164–173, 3 2017. [PubMed: 27992840]

[65]. Guan BO, Tam HY, Lau ST, and Chan HLW, "Ultrasonic hydrophone based on distributed Bragg reflector fiber laser," (in English), Ieee Photonics Technology Letters, vol. 17, no. 1, pp. 169–171, 1 2005.

[66]. Tseng YH and Wang JS, "Single-crystalline tellurite optical fiber hydrophone," Opt Lett, vol. 41, no. 5, pp. 970–3, 3 1 2016. [PubMed: 26974093]

[67]. Fay B, Ludwig G, Lankjaer C, and Lewin PA, "Frequency-Response of Pvdf Needle-Type Hydrophones," (in English), Ultrasound in Med. & Biol, vol. 20, no. 4, pp. 361–366, 1994. [PubMed: 8085292]

[68]. IEC 62127-3 Ultrasonics — Hydrophones — Part 3: Properties of hydrophones for ultrasonic fields up to 40 MHz, 2013.

[69]. Harris GR and Shombert DG, "A Pulsed near-Field Technique for Measuring the Directional Characteristics of Acoustic Receivers," (in English), IEEE Trans Son. Ultrason, vol. 32, no. 6, pp. 802–808, 1985.

[70]. Smith RA and Bacon DR, "A Multiple-Frequency Hydrophone Calibration Technique," (in English), J. Acoust. Soc. Am, vol. 87, no. 5, pp. 2231–2243, 5 1990. [PubMed: 2189922]

[71]. Conjusteau A, Ermilov SA, Su R, Brecht HP, Fronheiser MP, and Oraevsky AA, "Measurement of the spectral directivity of optoacoustic and ultrasonic transducers with a laser ultrasonic source," Rev Sci Instrum, vol. 80, no. 9, p. 093708, 9 2009. [PubMed: 19791945]

[72]. Guggenheim JA, Zhang EZ, and Beard PC, "A Method for Measuring the Directional Response of Ultrasound Receivers in the Range 0.3-80 MHz Using a Laser-Generated Ultrasound Source," (in English), IEEE Trans. Ultrason. Ferroelectr., Freq. Control, vol. 64, no. 12, pp. 1857–1863, 12 2017. [PubMed: 28976314]

[73]. Ayme EJ and Carstensen EL, "Cavitation Induced by Asymmetric Distorted Pulses of Ultrasound - Theoretical Predictions," (in English), IEEE Trans Ultrason Ferroelectr Freq Control, vol. 36, no. 1, pp. 32–40, 1 1989. [PubMed: 18284947]

[74]. Blackstock DT, "Connection between the Fay and Fubini solutions for plane sound waves of finite amplitude," J. Acoust. Soc. Am, vol. 14, no. 2, pp. 1019–1026, 1966.

[75]. Wear KA and Luo Y, "Considerations for choosing sensitive element size for needle and fiber-optic hydrophones II: Experimental validation of spatial averaging model," IEEE Trans Ultrason Ferroelectr Freq Control, vol. in press, 2018.

[76]. Soneson JE and Myers MR, "Gaussian representation of high-intensity focused ultrasound beams," J Acoust Soc Am, vol. 122, no. 5, pp. 2526–31, 11 2007. [PubMed: 18189543]

[77]. Muir TG and Carstensen EL, "Prediction of nonlinear acoustic effects at biomedical frequencies and intensities," Ultrasound Med Biol, vol. 6, no. 4, pp. 345–57, 1980. [PubMed: 7222267]

[78]. Du G and Breazeale MA, "Harmonic distortion of a finite amplitude Gaussian beam in a fluid," J Acoust Soc Am, vol. 80, no. 1, pp. 212–216, 1986.

[79]. Hamilton MF and Blackstock DT, Nonlinear Acoustics. San Diego, CA: Academic Press, 1998.

[80]. Averkiou MA and Hamilton MF, "Measurements of harmonic generation in a focused finite-amplitude sound beam," J Acoust Soc Am, vol. 98, no. 6, pp. 3439–42, 12 1995. [PubMed: 8550950]

[81]. Lucas BG and Muir TG, "The field of a focusing source," J. Acoust. Soc. Am, vol. 72, no. 4, pp. 1289–1296, 1982.

[82]. Goodman JW, Introduction to Fourier Optics. San Francisco: McGraw-Hill, 1968.

[83]. Carstensen EL, Law WK, McKay ND, and Muir TG, "Demonstration of nonlinear acoustical effects at biomedical frequencies and intensities," Ultrasound Med Biol, vol. 6, no. 4, pp. 359–68, 1980. [PubMed: 7222268]

[84]. Dalecki D, Carstensen EL, Parker KJ, and Bacon DR, "Absorption of finite amplitude focused ultrasound," J Acoust Soc Am, vol. 89, no. 5, pp. 2435–47, 5 1991. [PubMed: 1861004]

[85]. Sapozhnikov OA and Sinilo TV, "Acoustical field produced by a concave radiating surface with allowance for the diffraction," Acoustical Physics, vol. 48, no. 6, pp. 720–727, 2002.

[86]. Soneson JE, "Extending the Utility of the Parabolic Approximation in Medical Ultrasound Using Wide-Angle Diffraction Modeling," IEEE Trans Ultrason Ferroelectr Freq Control, vol. 64, no. 4, pp. 679–687, 4 2017. [PubMed: 28103552]

[87]. Bessonova OV and Wilkens V, "Membrane Hydrophone Measurement and Numerical Simulation of HIFU Fields up to Developed Shock Regimes," (in English), IEEE Trans. Ultrason. Ferroelectr., Freq. Control, vol. 60, no. 2, pp. 290–300, 2 2013. [PubMed: 23357903]

[88]. Ward B, Baker AC, and Humphrey VF, "Nonlinear propagation applied to the improvement of resolution in diagnostic medical ultrasound," J Acoust Soc Am, vol. 101, no. 1, pp. 143–54, 1 1997. [PubMed: 9000731]

[89]. IEC 62127-1 Ultrasonics – Hydrophones – Part 1: Measurement and characterization of medical ultrasonic fields up to 40 MHz, 2013.

[90]. Wilkens V and Molkenstruck W, "Broadband PVDF membrane hydrophone for comparisons of hydrophone calibration methods up to 140 MHz," (in English), IEEE Trans Ultrason Ferroelectr Freq Control, vol. 54, no. 9, pp. 1784–1791, 9 2007. [PubMed: 17941384]

[91]. Soneson JE, "A user-friendly software package for HIFU simulation," AIP Conference Proceedings, vol. 1113, pp. 165–169, 2009.

[92]. Gu J and Jing Y, "Modeling of wave propagation for medical ultrasound: a review," IEEE Trans Ultrason Ferroelectr Freq Control, vol. 62, no. 11, pp. 1979–93, 11 2015. [PubMed: 26559627]

[93]. Bacon DR, "Finite-Amplitude Distortion of the Pulsed Fields Used in Diagnostic Ultrasound," (in English), Ultrasound in Medicine and Biology, vol. 10, no. 2, pp. 189–195, 1984. [PubMed: 6390897]

[94]. Duncan T, Humphrey VF, and Duck FA, "A numerical comparison of nonlinear indicators for diagnostic ultrasound fields," Proceedings World Congress of Ultrasonics, pp. 85–88, 2003.

[95]. IEC/TS 61949 Ultrasonics - Field characterization - In situ exposure estimation in finite-amplitude ultrasonic beams, 2007.

[96]. Duck FA, "Estimating in situ exposure in the presence of acoustic nonlinearity," J Ultrasound Med, vol. 18, no. 1, pp. 43–53, 1 1999. [PubMed: 9952079]

[97]. Bigelow TA and O'Brien WD, "Experimental evaluation of indicators of nonlinearity for use in ultrasound transducer characterizations," (in English), Ultrasound in Medicine and Biology, vol. 28, no. 11-12, pp. 1509–1520, Nov-Dec 2002. [PubMed: 12498947]

[98]. Beard PC, Hurrell AM, and Mills TN, "Characterization of a polymer film optical fiber hydrophone for use in the range 1 to 20 MHz: A comparison with PVDF needle and membrane hydrophones," (in English), IEEE Trans Ultrason Ferroelectr Freq Control, vol. 47, no. 1, pp. 256–264, 1 2000. [PubMed: 18238538]

[99]. Reilly CR and Parker KJ, "Finite-amplitude effects on ultrasound beam patterns in attenuating media," J Acoust Soc Am, vol. 86, no. 6, pp. 2339–48, 12 1989. [PubMed: 2600313]

[100]. Cherin EW, Poulsen JK, van der Steen AF, Lum P, and Foster FS, "Experimental characterization of fundamental and second harmonic beams for a high-frequency ultrasound transducer," Ultrasound Med Biol, vol. 28, no. 5, pp. 635–46, 5 2002. [PubMed: 12079700]

[101]. Weber M and Wilkens V, "Using a heterodyne vibrometer in combination with pulse excitation for primary calibration of ultrasonic hydrophones in amplitude and phase," (in English), Metrologia, vol. 54, no. 4, pp. 432–444, 8 2017.

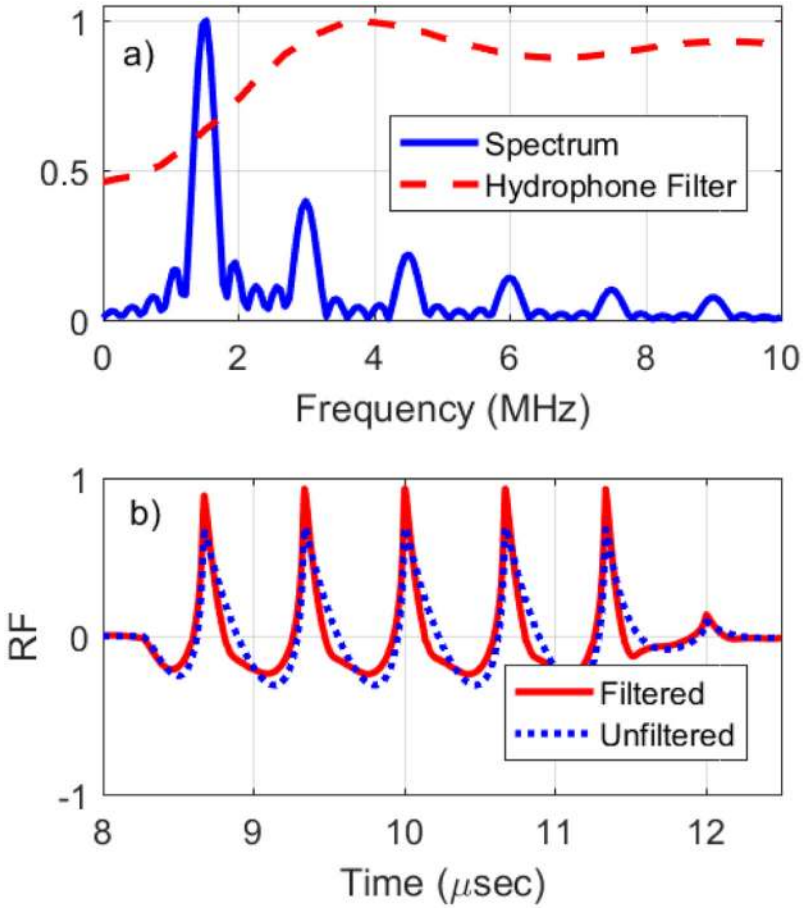


**Fig. 1.**

a) spectrum of a nonlinear signal (solid line) and hydrophone frequency-dependent sensitivity (dash line). b) unfiltered waveform (dotted line) and waveform distorted by hydrophone (solid line). The hydrophone boosts harmonics relative to the fundamental, resulting in a waveform with reduced rarefactional pressure and exaggerated high-frequency content, which is manifested as sharper, taller, compressional peaks.

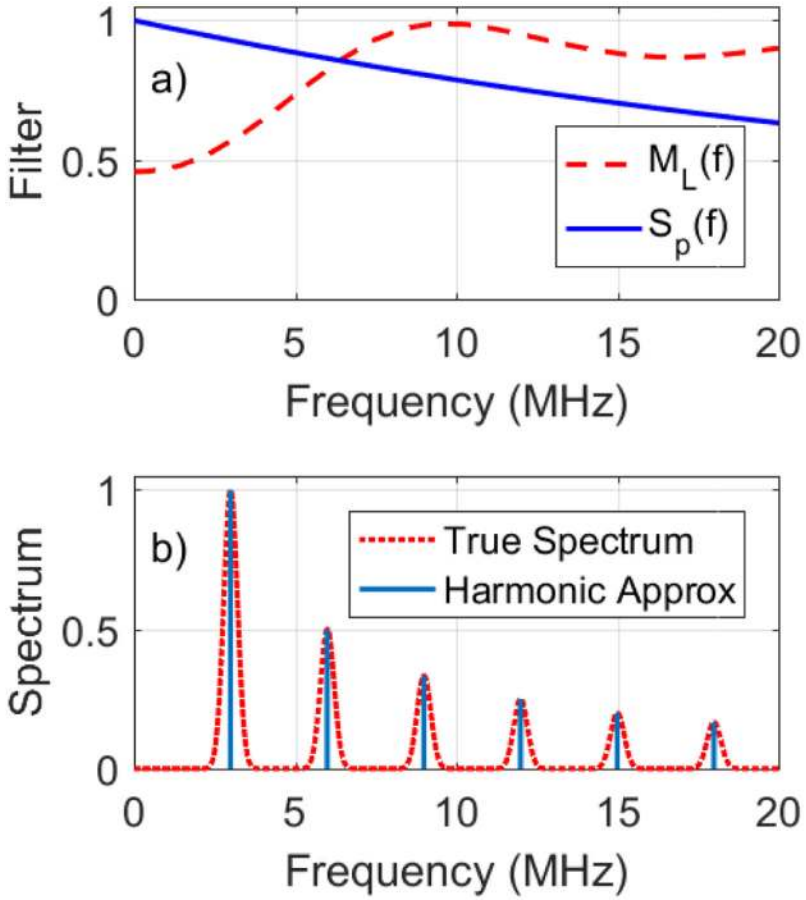


**Fig. 2.**

a) Theoretical sensitivity filter, $M_L(f)$, (red dashed line) and spatial averaging filter, $S_p(f)$ (solid blue line), b) Model true spectrum (red dotted line) and harmonic approximation (blue solid line).

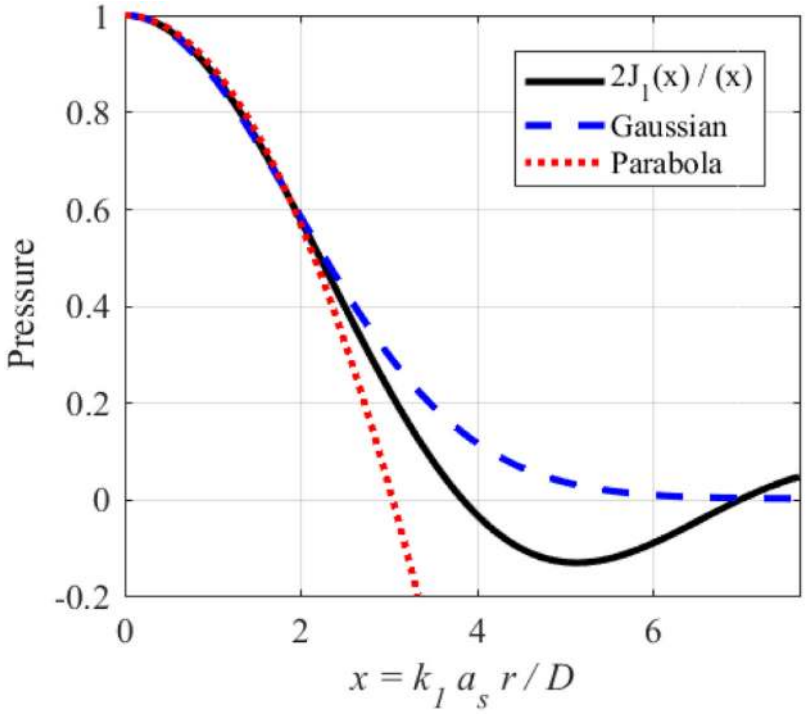


**Fig. 3.**

Gaussian and parabolic approximations to radial diffraction pattern for the fundamental frequency component where $k_1 = 2\pi/\lambda_1$, $\lambda_1 = c/f_1$, $c$ = speed of sound, $a_s$ = the radius of the source, and $D$ = the focal length of the source. Both approximations are accurate for radial coordinate < half width half maximum (HWHM) of the beam.

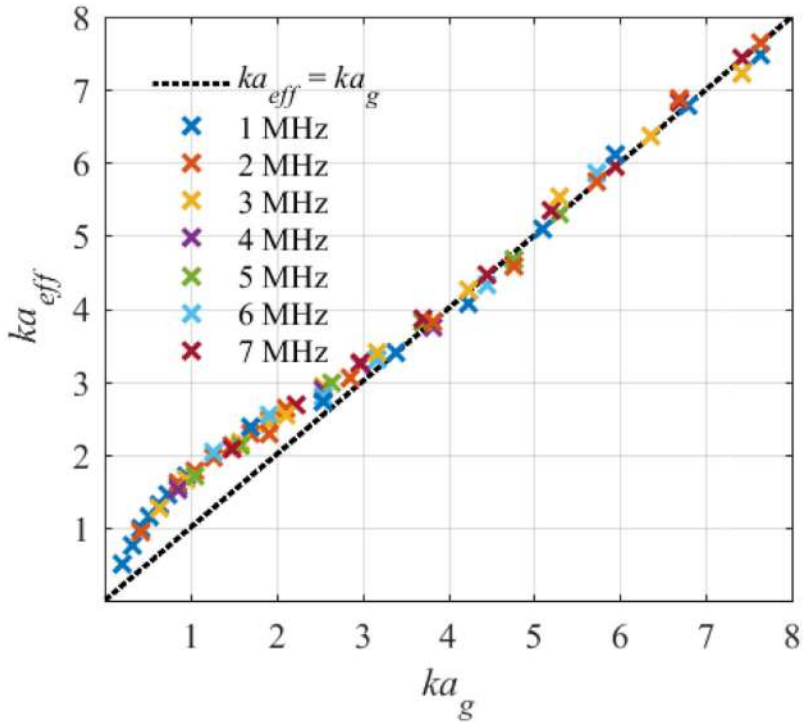


**Fig. 4.**

Scatter plot of $ka_{eff}$ estimated from RB model directivity, $2J_1(ka\sin\theta) / ka\sin\theta$ vs. $a_g$ for a needle hydrophone that obeys the RP model, $H(\rho, f)$ with $a_1 = a_2 = a_g$. The effective radius, $a_{eff}$, was chosen by selecting the value of $a$ that minimized RMSD between the two models. The angle range for the directivity fit was $-60° < \theta < 60°$.

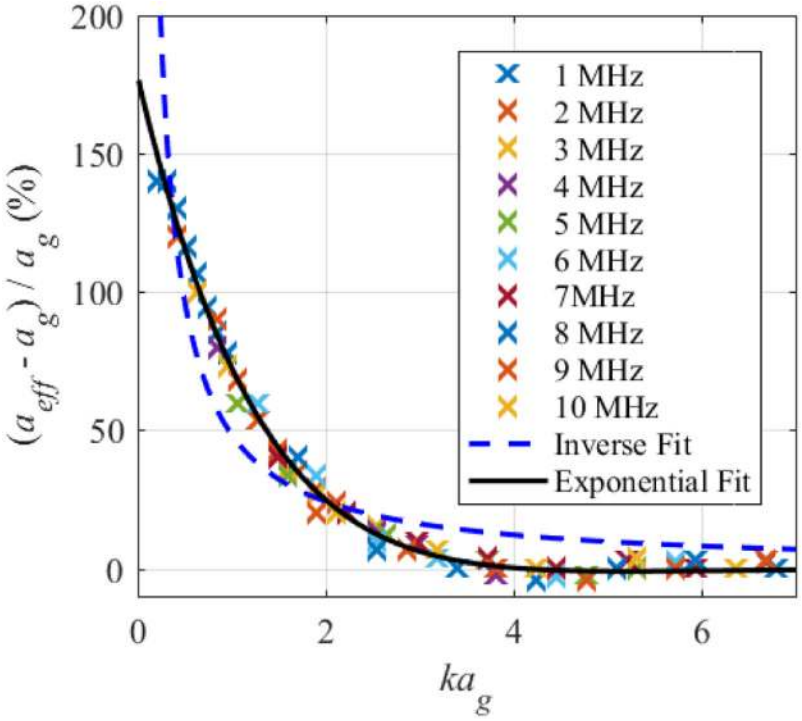


**Fig. 5.**

Relative difference between $a_{eff}$ and $a_g$ plotted as a function of $ka_g$. The root mean square difference (RMSD) between fit and data is lower for the exponential fit than the inverse fit. The angle range for the directivity fit was $-60° < \theta < 60°$.

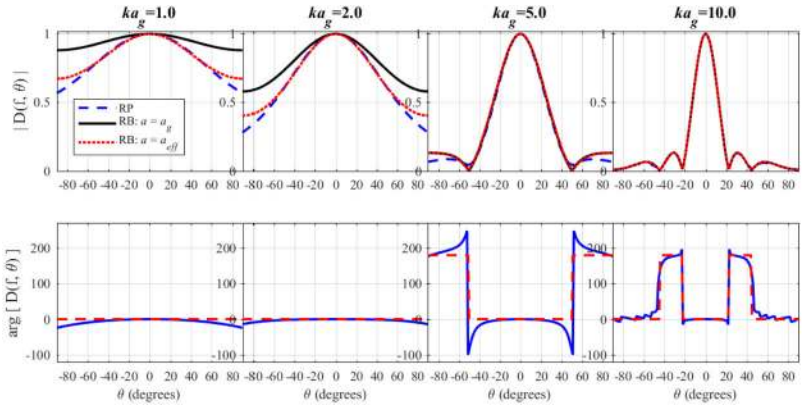


**Fig. 6.**

Magnitude and phase of directivity functions for four values of $ka_g$ for the rigid piston (RP) model evaluated for $a_1 = a_2 = a_g$ and two versions of the rigid baffle (RB) model evaluated for $a = a_g$ and $a_{eff}$. The angle range for the directivity fit was $-60° < \theta < 60°$.

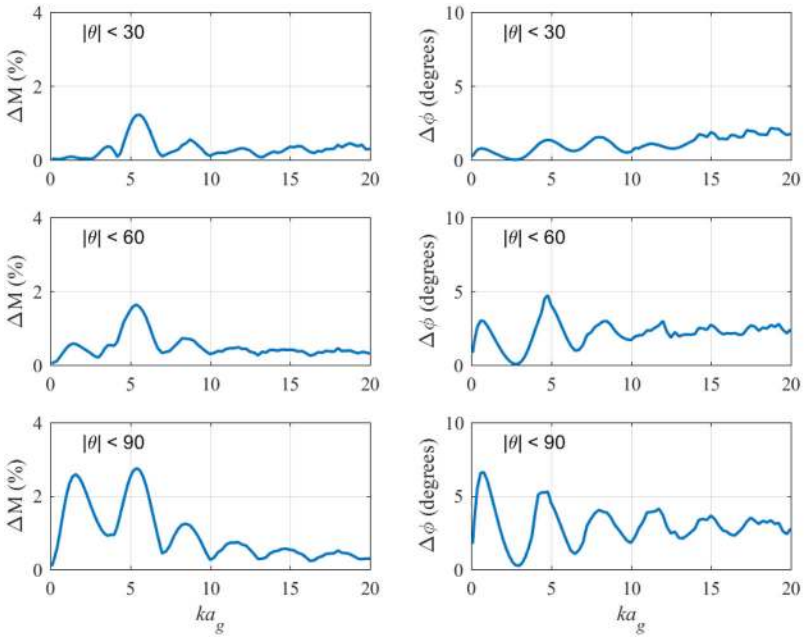


**Fig. 7.**

Differences in magnitude and phase between the RP model directivity evaluated for $a_1 = a_2 = a_g$ and RB model directivity evaluated for $a = a_{eff}(f)$.

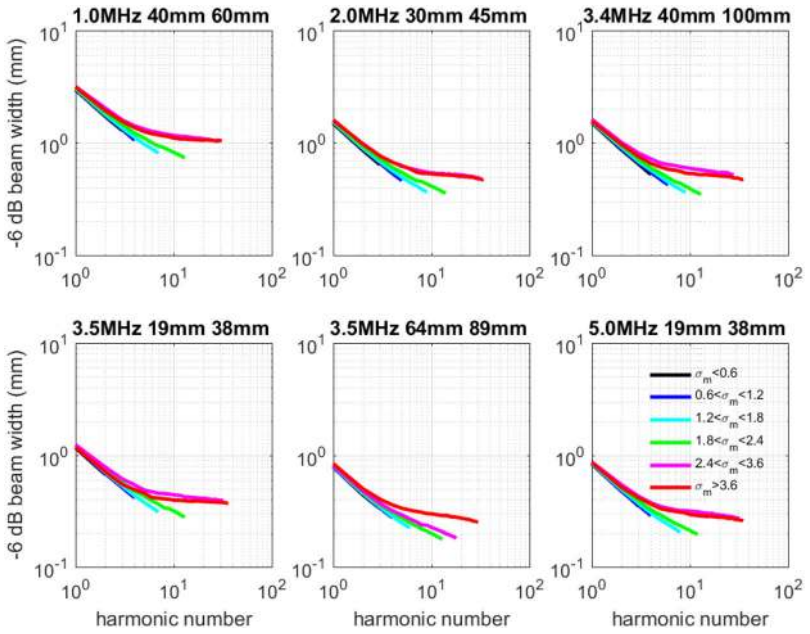


**Fig. 8.**

−6 dB beam width (FWHM) vs harmonic number for six transducers. The title above each plot gives center frequency, diameter, and focal length. The symbol $\sigma_m$ refers to the nonlinear propagation parameter. The threshold for approximate power law dependence of FWHM vs. harmonic number (straight line on log log plot) is $\sigma_m < 2.4$ ($\sigma_q < 3$) for the six transducers investigated.

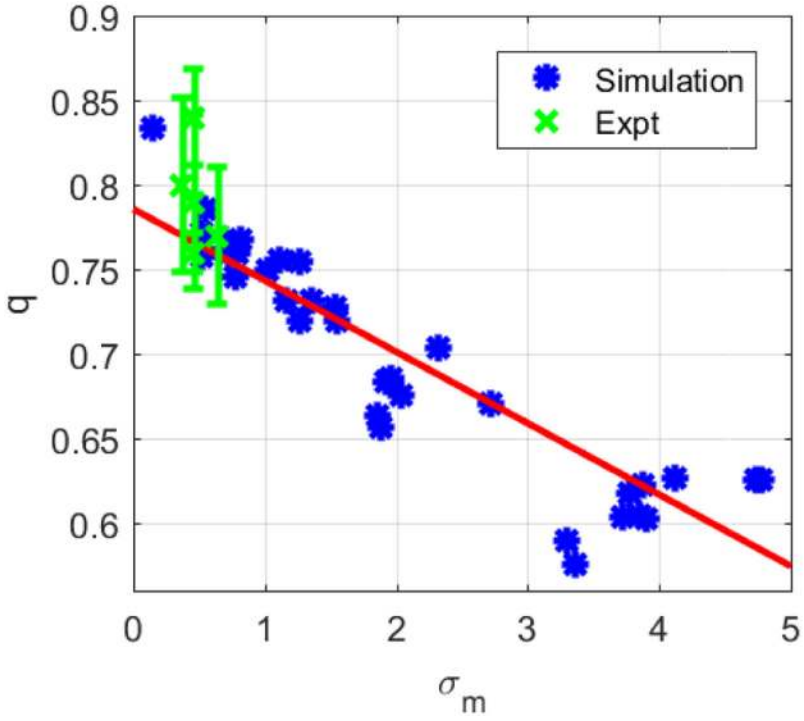


**Fig. 9.**

Simulation and experimental results for exponent for power law dependence (based on the first 5 harmonics) of FWHM vs nonlinear propagation parameter $\sigma_m$. A least-squares linear fit is shown (red line).

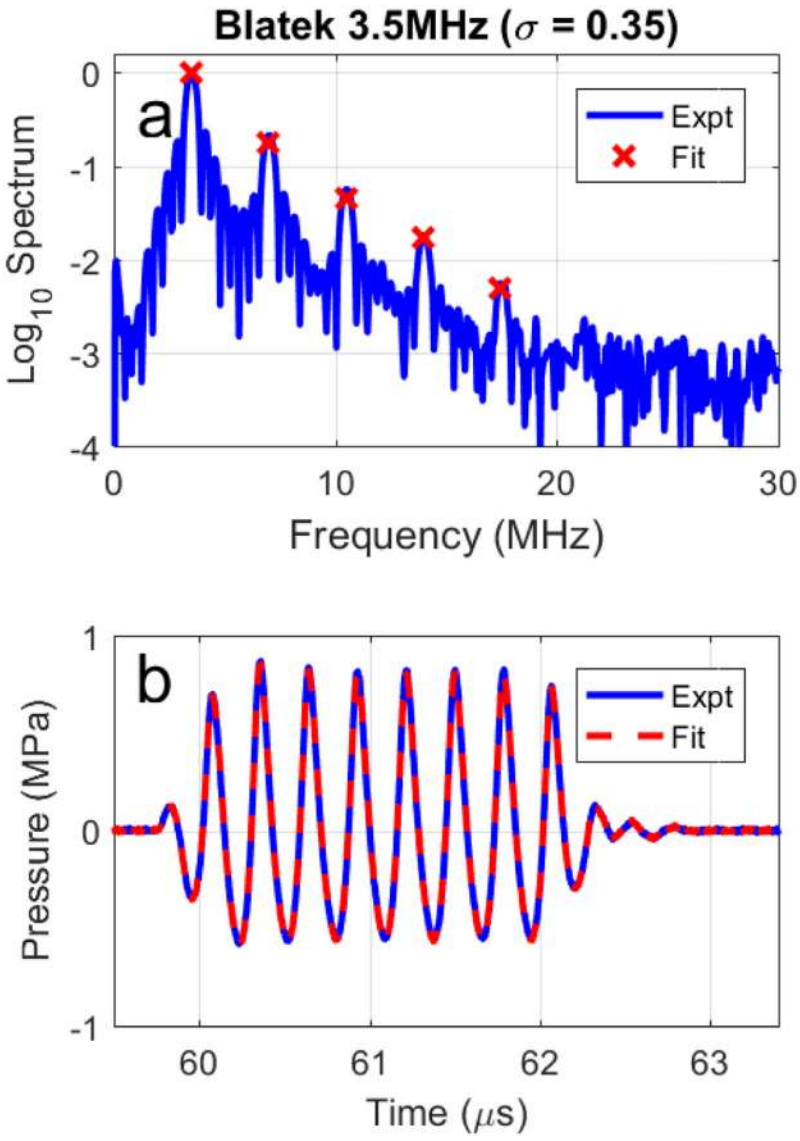


**Fig. 10.**

Hydrophone measurements at the focus of the Blatek 3.5 MHz transducer. a) Spectrum. Measurement is shown in the blue line. Fits to harmonic strengths based on spectra with relative harmonic strengths according to Blackstock's theory are shown in red x's. b) time-domain radio-frequency (RF) signal. Measurement is shown in the blue line. A best-fit signal with relative harmonic strengths corresponding to Blackstock's theory with $\sigma = 0.35$ is shown in the red dashed line.

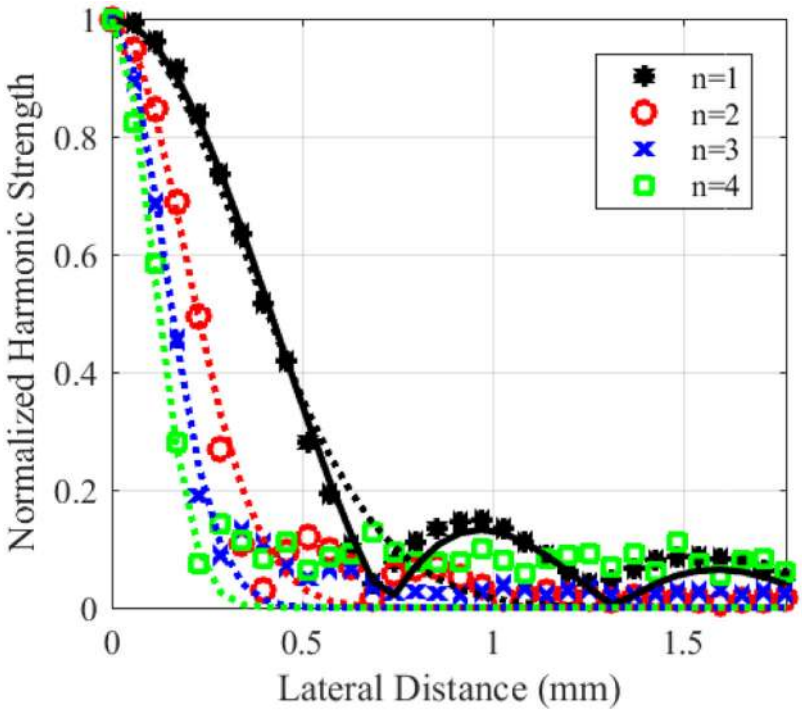


**Fig. 11.**

Lateral beam scans for harmonics of Blatek transducer operated at 3.5 MHz. The solid black line shows the theoretical lateral profile at the fundamental frequency. The dotted lines show Gaussian fits for the fundamental and harmonics based on a model in which HWHM is proportional to $1 / n^{[}$ and $n$ = harmonic number. The harmonics show approximately Gaussian behavior at least up to radial distances of 0.5 mm, corresponding to a maximum hydrophone diameter of 1 mm and therefore suggesting relevance to most hydrophones used in ultrasonics.

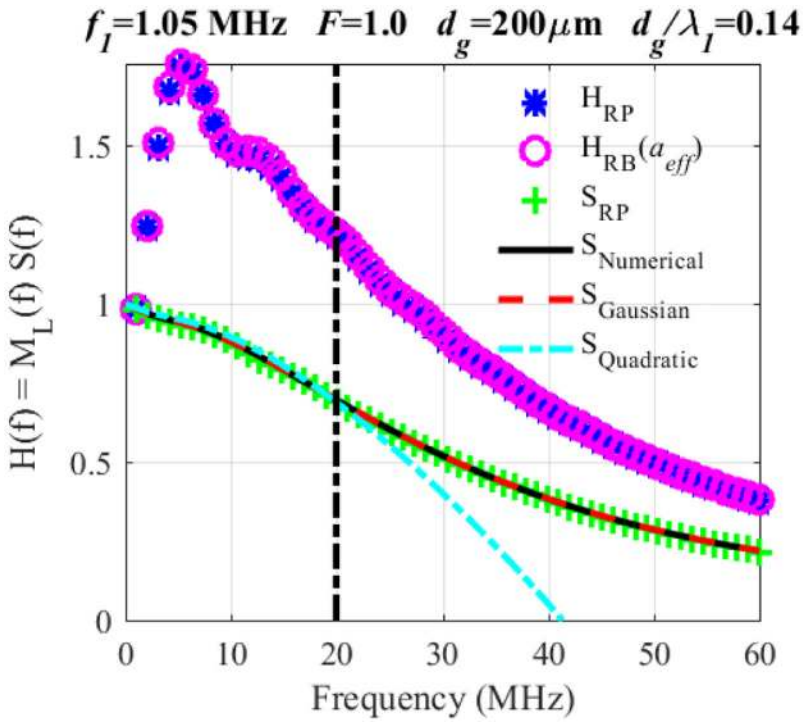


**Fig. 12.**

RP and RB hydrophone transfer functions $H_{RP}(f)$ (with $a_1=a_2=a_g$) and $H_{RB}(f)$ with $a= a_{eff}(f)$, RP spatial averaging filter $S_{RP}(f) = H_{RP}(f) / M_L(f)$, and numerical, Gaussian, and quadratic forms for the spatial averaging filter, $S_{Numerical}(f)$ (17), $S_{Gaussian}(f)$ (20), and $S_{Quadratic}(f)$ (30). Transducer parameters are for the Sonic Concepts H101 transducer operated at its lower frequency option of 1.05 MHz. The hydrophone sensitive element geometrical diameter was 200 μm. The vertical chain-dash line gives the limit predicted by (33) of the validity of the quadratic approximation for the spatial averaging filter given by (30).

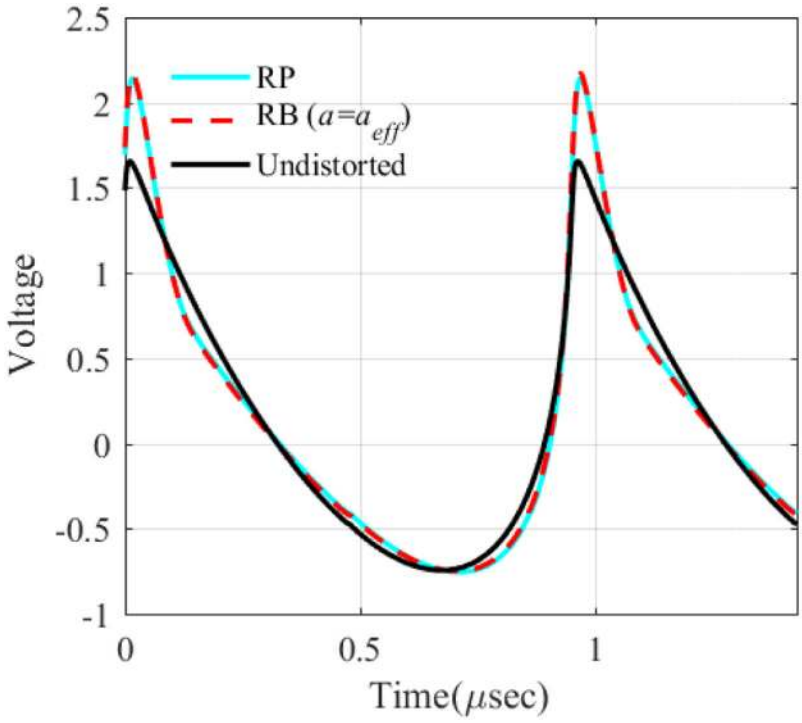


**Fig. 13.**

Simulated hydrophone output voltage for a tone burst produced by the Sonic Concepts H101 transducer operated at its lower frequency option of 1.05 MHz. The hydrophone sensitive element geometrical diameter was 200 μm. Voltage is in arbitrary units.

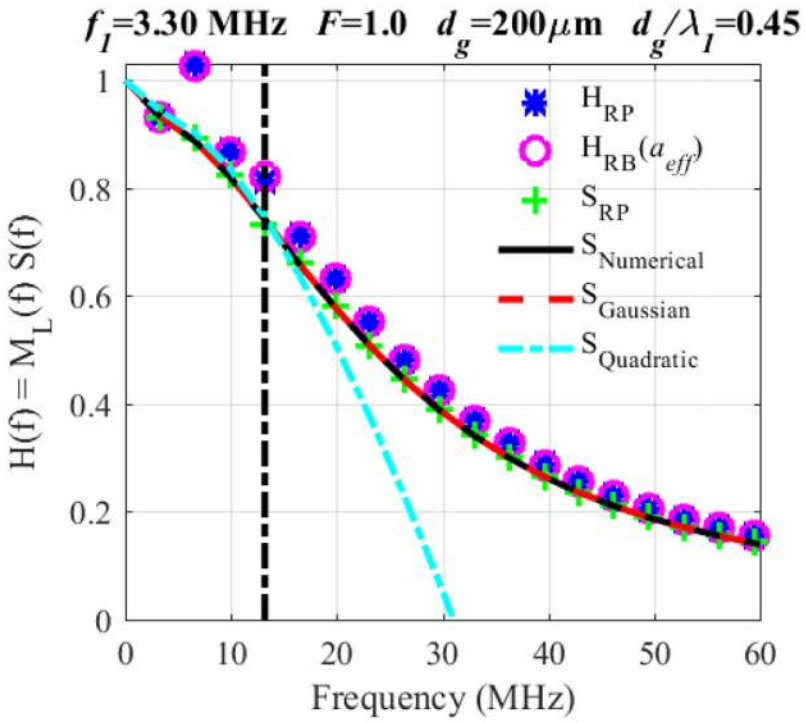


**Fig. 14.**

RP and RB hydrophone transfer functions $H_{RP}(f)$ (with $a_1=a_2=a_g$) and $H_{RB}(f)$ with $a= a_{eff}(f)$, RP spatial averaging filter $S_{RP}(f) = H_{RP}(f) / M_L(f)$, and numerical, Gaussian, and quadratic forms for the spatial averaging filter, $S_{Numerical}(f)$ (17), $S_{Gaussian}(f)$ and $S_{Quadratic}$(f) (30). Transducer parameters are for the Sonic Concepts H101 transducer operated at its higher frequency option of 3.30 MHz. The hydrophone sensitive element geometrical diameter was 200 μm. The vertical chain-dash line gives the limit predicted by (33) of the validity of the quadratic approximation for the spatial averaging filter given by (30).

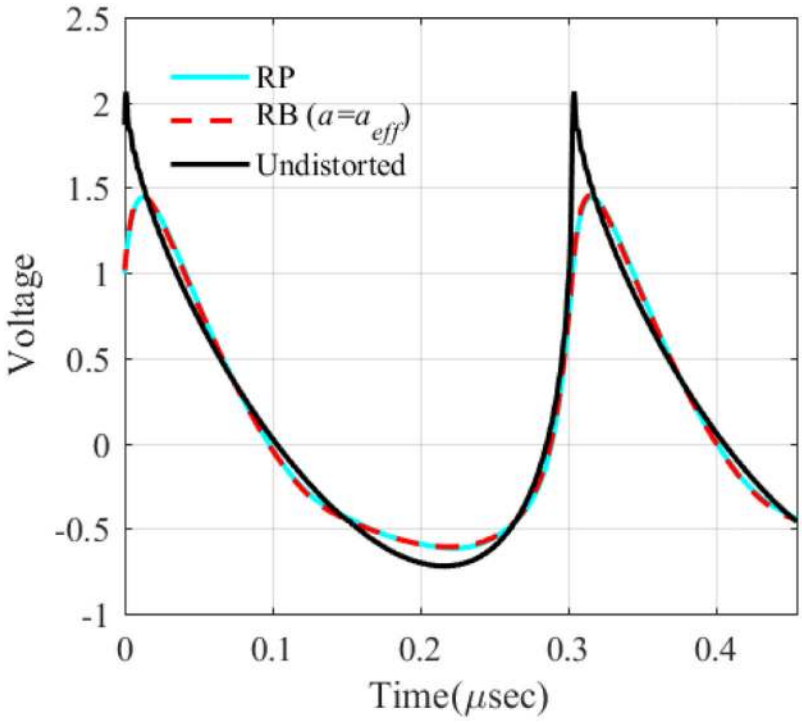


**Fig. 15.**

Simulated hydrophone output voltage for a tone burst produced by the Sonic Concepts H101 transducer operated at its higher frequency option of 3.30 MHz. The hydrophone sensitive element geometrical diameter was 200 μm. Voltage is in arbitrary units.

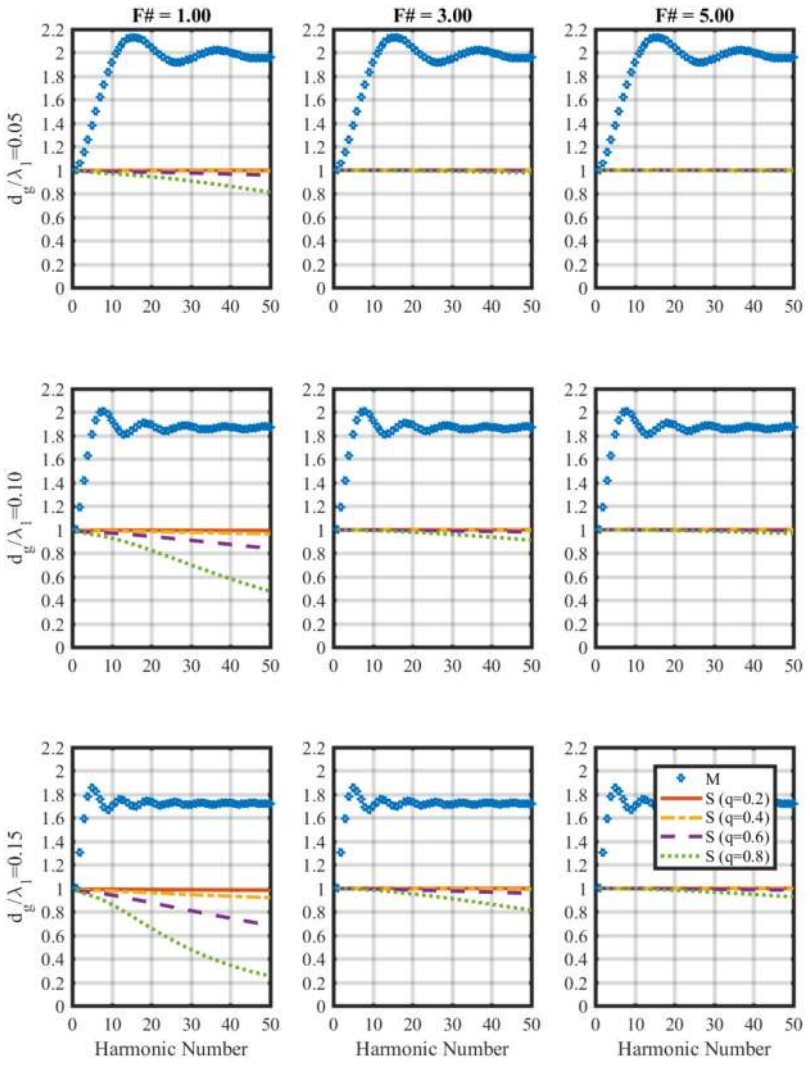


**Fig 16.**

Graphical Guide for hydrophone spatiotemporal response. M: hydrophone sensitivity. S: spatial averaging filter. Total spatiotemporal transfer function = MS. $d_g$: geometrical sensitive element diameter, $\lambda_1$: wavelength of fundamental component. *F*#: ratio of transducer focal length to diameter. M is normalized to its value at the fundamental frequency. Note that M can vary from theory, especially for frequencies above the frequency corresponding to the maximum theoretical sensitivity, due to hydrophone design complexities not captured by the RP model. Spatial averaging filter depends on *q*, which determines the dependence of harmonic beam width on harmonic beam number. See text for details.

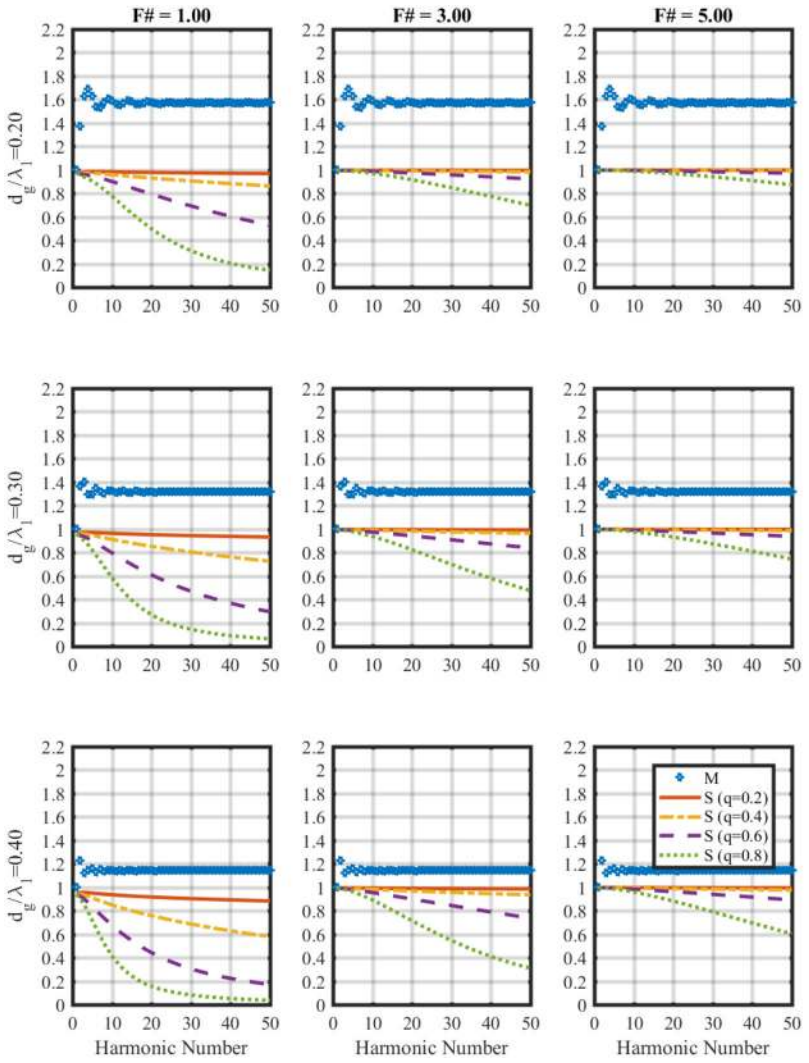


**Fig 17.**

Graphical Guide for hydrophone spatiotemporal response. M: hydrophone sensitivity. S: spatial averaging filter. Total spatiotemporal transfer function = MS. $d_g$: geometrical sensitive element diameter, $\lambda_1$: wavelength of fundamental component. *F*#: ratio of transducer focal length to diameter. M is normalized to its value at the fundamental frequency. Note that M can vary from theory, especially for frequencies above the frequency corresponding to the maximum theoretical sensitivity, due to hydrophone design complexities not captured by the RP model. Spatial averaging filter depends on *q*, which determines the dependence of harmonic beam width on harmonic beam number. See text for details.

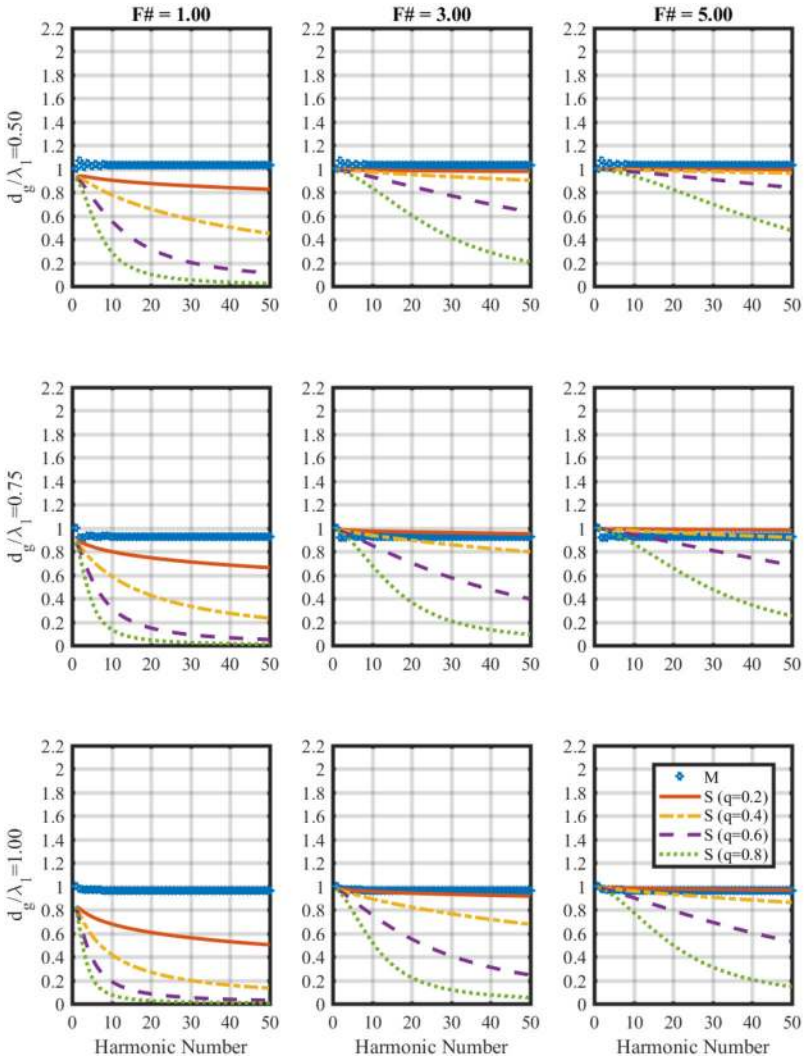


**Fig 18.**

Graphical Guide for hydrophone spatiotemporal response. M: hydrophone sensitivity. S: spatial averaging filter. Total spatiotemporal transfer function = MS. $d_g$: geometrical sensitive element diameter, $\lambda_1$: wavelength of fundamental component. *F*#: ratio of transducer focal length to diameter. M is normalized to its value at the fundamental frequency. Note that M can vary from theory, especially for frequencies above the frequency corresponding to the maximum theoretical sensitivity, due to hydrophone design complexities not captured by the RP model. Spatial averaging filter depends on *q*, which determines the dependence of harmonic beam width on harmonic beam number. See text for details.

**TABLE I**

VALIDITY OF DIFFRACTION FORMULA FOR H-101

| **Criterion** | **Frequency:** | **1.05 MHz** | **3.3 MHz** |
|---|---|---|---|
| $k_1 a_s >> 1$ [71] | $k_1 a_s$ | 143 | 448 |
| | Criterion met? | Yes | Yes |
| $\sin^2 \alpha_0 << 2$ [71] | $\sin^2 \alpha_0$ | 0.26 | 0.26 |
| | Criterion met? | Yes | Yes |
| $\sin^3 \alpha_0 << 16\pi / (k_1 a_s)$ [71] | $\sin^3 \alpha_0$ | 0.13 | 0.13 |
| | $16\pi / (k_1 a_s)$ | 0.35 | 0.11 |
| | Criterion met? | Yes | No |
| FWHM theory (mm) | | 1.95 | 0.62 |
| FWHM simulate (mm) [76] | | 1.92 | 0.62 |
| FWHM expt (mm) [13] | | 1.97 | 0.63 |

Numbers based on Sonic Concepts H-101: $a_S = 32$ mm, $D = 62.6$ mm, $F\# = D/(2a_S) = 1$, $\sin \alpha_0 = a_S / D$. Theoretical FWHM = $1.41 \lambda_1 F\#$.

**TABLE II**

TRANSDUCER PARAMETERS

| **Manufacturer** | **Diameter (mm)** | **Focal Length (mm)** | **Center / Driving Frequency (MHz)** | ***q*** | **Simulation or Experiment** |
|---|---|---|---|---|---|
| - | 40 | 60 | 1 / 1 | | Simulation |
| - | 30 | 45 | 2 / 2 | | Simulation |
| Sonic Concepts | 40 | 100 | 3.4 / 3.4 | | Simulation |
| Blatek | 63.5 | 88.9 | 3.5 / 2.5 | 0.80 ± 0.09 | Experiment |
| | | | 3.5 / 3.5 | 0.84 ± 0.05 | Both |
| | | | 3.5 / 4.5 | 0.77 ± 0.07 | Experiment |
| Panametrics | 19.1 | 38.1 | 3.5 / 3.5 | 0.76 ± 0.02 | Both |
| Panametrics | 19.1 | 38.1 | 5 / 5 | 0.79 ± 0.09 | Both |

**TABLE III**

PARAMETRIC FITS FOR $(a_{eff} - a_g) / a_g$.

| **Angle Range** (°) | $\mathbf{Ae^{-Bka_g}}$ | | | $\frac{C}{ka_g}$ | | |
|---|---|---|---|---|---|---|
| | **A** | **B** | **RMSD (%)** | **C** | **95% CI** | **RMSD (%)** |
| \|θ\| < 10 | 1.81 | 1.07 | 3.2 | 0.44 | 0.41 – 0.48 | 14.8 |
| \|θ\| < 20 | 1.87 | 1.09 | 3.3 | 0.45 | 0.42 – 0.49 | 15.5 |
| \|θ\| < 30 | 1.85 | 1.05 | 3.2 | 0.46 | 0.42 – 0.50 | 16.1 |
| \|θ\| < 40 | 1.84 | 1.02 | 3.3 | 0.47 | 0.43 – 0.51 | 16.8 |
| \|θ\| < 50 | 1.86 | 1.02 | 3.8 | 0.47 | 0.43 – 0.51 | 13.9 |
| \|θ\| < 60 | 1.90 | 0.99 | 4.2 | 0.49 | 0.45 – 0.53 | 18.6 |
| \|θ\| < 70 | 1.96 | 0.96 | 5.1 | 0.51 | 0.46 – 0.56 | 20.9 |
| \|θ\| < 80 | 2.07 | 0.96 | 3.9 | 0.54 | 0.50 – 0.59 | 20.7 |
| \|θ\| < 90 | 2.13 | 0.94 | 4.5 | 0.57 | 0.52 – 0.62 | 22.5 |